ISSN: 3066-3938

Review Article

Thermodynamics Research: Open Access

Quantitative Simulations on Temperature-Dependent Lattice Thermal Capacity of Linear, Branched and Cyclic Polymers

Valeri Ligatchev*

Independent researcher, Singapore

***Corresponding Author**
Valeri Ligatchev, Independent researcher, Singapore.

Submitted: 2026, July 21; **Accepted**: 2026, Aug 24; **Published**: 2026, Sep 02

Citation: Ligatchev, V. (2026). Quantitative Simulations on Temperature-Dependent Lattice Thermal Capacity of Linear, Branched and Cyclic Polymers. *Ther Res: Open Access, 3*(1), 01-40.

Abstract

Effects of spatial confinement, and interactions among neighboring molecular fragments, as well as amendments in topological characteristics are taken into account explicitly at semi-empirical quantitative evaluations on temperature-dependent isochoric lattice thermal capacity of several one-dimensional (linear), branched and 'cyclic' polymeric macromolecules, in order to replicate compellingly their experimentally obtained temperature-dependent isobaric counterparts. Those experimental dependencies might exhibit 'sublinear', nearly-linear, and 'super-linear' enlargement(s) with the temperature within 'moderate' temperature ranges alongside with so-called 'low-temperature anomalies', which are persistently manifested in profound decline(s) in the lattice thermal capacities with the temperature diminishment below the 'moderate' ranges. The obtained lengths of the spatial confinement of acoustic phonons located within the liner and branched polymers are compared with the Kuhn and persistent lengths of the linear, branched and cyclic polymers, while other simulation results are discussed in comparison with predictions of the 'fractal theory' of heat capacity of polymers, Tarasov's equations, as well as with those of the 'free energy of confinement' approximation.

Keywords: Harmonic, Anharmonic, Thermal, Capacity, Low-Dimensional, Polymers

1. Introduction

Physical properties of polymeric solids comprised of linear (1D), branched, two-dimensional, 2D, and 3D macromolecules are of key importance for many of their essential application areas: materials engineering and science, medical and biomedical usages, chemistry, etc. Those polymeric solids are customarily comprised of adjoined *repetitive* (monomeric) molecular units, aggregated into *macromolecules*, though – in general – their atomic structure(s) might appear either in *crystalline* and/or *amorphous* (glassy) modifications, or even as a combination of those [1-3]. Structural and topological characteristics of individual macromolecules (chains) are of primarily importance for the *linear* 'molecular wires' (MWs), quasi-crystals comprised of (interacting) 1D MWs, and even for branched polymers, whereas for the 2D and 3D polymeric solids, planar and spatial interconnections among their macro-molecules as well as morphological characteristics of entire solids (e.g., their shape, sizes, crystalline orientation – if any) might be of crucial significance as well. Therefore, structural, topological and statistical characterization of linear, branches and globular macro-molecules (MWs) became attractive scientific topic in the second half of the twenty's century.

In particular, both before beginning and especially soon after ending of the World War II, intensive experimental and theoretical investigations on the structural, mechanical, energetic, thermal, and others fundamental characteristics of polymers yielded in several celebrated theoretical concepts: freely joint and freely-rotating ideal chain ones, hindered rotation model, rotational isomeric state model, warm-like (Kratky-Porod) chain model, Flory's characteristic ratio(s) (FCRs) and length, Kuhn length (KL), which is representing 'statistical segment' in a polymer chain (MW), and '…characterizing crossover to the large-scale random-walk behavior…', persistence

length (PL), which is the '…distance over which orientations of the bonds persists…', radius of gyration (RG), excluded volume and self-avoiding walk, Stockmayer-Hecht model (and its Genensky-Newel extension) for vibrational spectrum of 1D crystals with *realistic* phonon dispersion, and 'embedded' *interactions* among neighboring MWs, as well as Tarasov's equations for thermal capacity of layered and chain polymeric structures, alongside with others fundamental models closely related to them [4-10]. Extended discussion(s) on archetypal features of some of the aforementioned approximations are provided in the *second section*. Though those approximations rather represent *idealized* structural, topological, and spectral characteristics of low-dimensional polymeric materials, they became tremendously beneficial for deep understanding and appropriate interpretations of many key physical concepts and properties of both real and idealized chain and branched polymers with essentially different spatial extents (lengths) and topology (connectivity) among their monomers and macromolecules.

Though aforementioned spatial characteristics of idealized solid and liquids polymers comprise '…wide range…' of their physically meaningful specific lengths, those characteristics customarily do not include explicitly length (spatial extent) of the *confinement* of thermal acoustic and optical vibrations (phonons), in spite of its very obvious significance for various *thermal* characteristics of polymeric materials. For instance, key features of *thermal transport* in high-quality *bulk* crystalline semiconductors and insulators are defined evidently by the phonon-phonon *interactions*, while phonon scattering on point and linear defects might affect considerably parameters of thermal transport in real semiconductors and insulators as well [7,11,12]. In other words, phonon(s) Mean-Free-Path (MFP) – or their 'coherence length' – became among the key *characteristic lengths* of those *bulk* material, while so-called 'Casimir length' (CL)– which apparently simply coincides with the (appropriate) *spatial extent* of nano-crystals, nano-flakes, nano-ribbons, nano-wires, 'quantum dots', etc. – came to be of key importance for thermal transport of aforementioned *nano-scaled* materials [13-15].

Nonetheless, it is not very clear even up to now, which of the mentioned above (and discussed briefly, for instance, elsewhere in ref. [7] .) well-established *structural* (topological, morphological) characteristic *lengths* of idealized and real linear polymers as well as those of branched ones actually defines their MFP and/or *confinement* length of their acoustic and optic phonons? Furthermore, those confinement lengths (spatial extents) – alongside with other purely 'geometrical' characteristics of inter-chain interactions in 1D polymeric quasi-crystals – affect very straightforwardly particularities of other crucial (for thermal transport and heat capacity) features of those polymers: their Vibrational Density-Of-States (VDOS) functions, phonon dispersion relation(s), etc. This misapprehension impedes considerably appropriate understanding of some intriguing features of experimentally evaluated dependencies on isobaric thermal capacities of real linear and branched polymers: tenacious appearance of so-called 'low-temperature' anomalies [16] (see also references therein), as well as those of 'sub-linear' and 'super-linear' enlargement with the temperature within moderate temperature ranges, etc. [7-9,16,17]. Those common features might be manifested as well in similar dependencies of the *real* linear and branched polymers composed of essentially different structural 'blocks': e.g., 'aromatic' and (for instance) '5-member' and/or '7-member' rings, different types of the 'backbone' chains, 'terminal groups', with and without incorporated oxygen and nitrogen atoms, etc.: see some discussion on this issue with particular examples of those polymers in the second section.

This article is predominantly devoted to semi-empirical simulations and, detailed discussion(s) on effect(s) of alteration(s)s in key structural, topological and morphological features of linear and branched polymers as well as of changes in their other key physical characteristics on the modelled temperature-dependent heat capacity and comparison of those simulated dependencies with their experimental counterparts reported for several different types (linear, branched, cyclic) of real polymeric materials. Details of implemented simulation approach are described at the beginning of the third section of the article.

Obtained simulation results (also presented and discussed in the third and fourth sections of this article), intend to clarify some outstanding issues on the actual *physical* significance of the mentioned above in this section renowned theoretical approximations and their connection(s) to the structural, topological, morphological, and spectral features on the thermal characteristics of real linear and branched polymers [1-10]. In particular, intimate interrelation among amendments in length of spatial confinement of quantized vibrations (phonons) in those real linear, branched and cyclic polymers, and, especially, particularities of their simulated and experimental temperature-dependent thermal capacity, will be discussed (to some extent) in connections with the well-documented changes in the mentioned above renowned structural and statistical characteristics of those low-dimensional polymers. Thus, combination of aforementioned well-established theoretical approximations, with more realistic (and yet innovative) simulation techniques is generally expected not only allow one to replicate convincingly representative features of the experimental temperature dependencies of their lattice heat capacities in wide temperature ranges, but also articulate crucial physical parameters and key spatial extents of those well-known structural models in order to clarify further their fundamental essences in a wider physical context, protracted well beyond their original (i.e., predominantly classical, 'geometrical' and/or statistical) meanings [7,16].

2. Some Archetypal Structural and Morphological Models of Low-Dimensional Polymers

Mentioned in the previous section '*standard*' structural model(s) of *linear* polymer(s) might be (formally) separated into two groups: those linked (in one or another ways) to *real* 'discrete' *atomic* and/or *molecular* structures of their monomers (molecular units), and essentially idealized *continuous* models [1-3]. Aforementioned differences are crucial for 'flexibility mechanisms' and/or those of *conformation* of linear and branched polymeric chains (MWs) with dominant rotations of 'discrete' inter-atomic bonds around elongated spatial direction(s) of linear chains (i.e., variation in *torsion* angles) for the first group, or bending of entire *continuous* chain on (for instance) a 2D plane. It is noteworthy, that both aforementioned models are 'composed' rather based on the idealized *continuous* representation(s) of the 'backbone' and 'branch' chains, than on their more realistic 'discrete' (atomistic) representation(s) [1].

2.1. 'Standard' Structural and Topological Models of Linear and Branched Polymers

The Figures 1(a), and 1(b) illustrate key features of two well-known 'representatives' from the first and second aforementioned groups. The Figures 1(c) and 1(d) also illustrate key features of the 'comb' and 'bottle-brash' models of the *branched* polymers [1-3]. One of the most important spatial extents of the 'freely joint' model (with *no interactions* among joint *linear* fragments and no correlation among directions of chemical bonds between such joined fragments) is so-called 'Kuhn length', L_K, (see also Figure 1(a) for illustration), corresponding to the length of a *rigid* 'statistical segment' in a freely joint polymer chain (or molecular wire, MW), with its rigidity defined by the FCR [1-5]. In contrast, the Kratky-Porod (KP) model is rather characterized by the '*persistence*' length, L_p, and the curvature radius, *R* (see Figure. 1(b)), which – in a general case – may *vary* at every point of a continuous chain. Both L_p and *R* quantities are characterizing *stiffness* of the quasi-continuous polymeric chain (MW), while the *dimensionless* Flory characteristic ratio(s), C_n, alongside with the Flory length, L_F, rather characterize stiffness of particular linear segments within framework of the freely 'jointed' chain model [1-3]. Well-known structural (topological) models of the *branched* polymers, the 'comb' and 'bottle-brash' ones are sketched in the Figures 1(c), (d) [1-3].

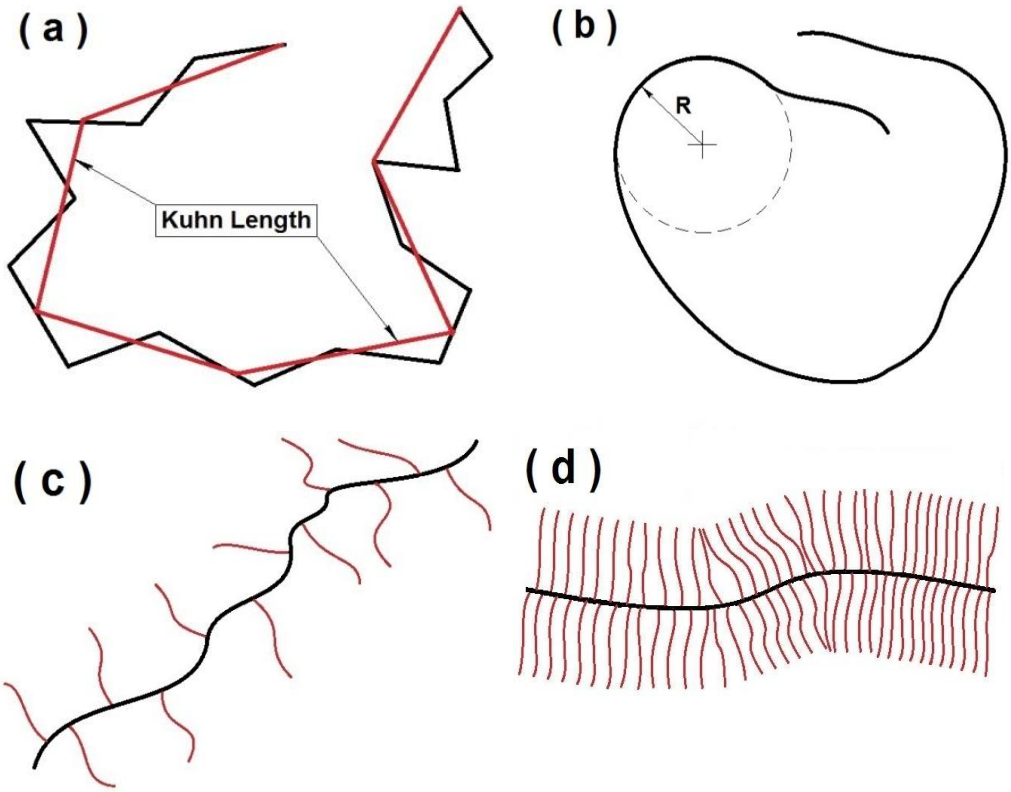

Figures 1(a), 1(b), 1(c), 1(d): (color online). Two-dimensional sketches of some well-known models of the linear and branched polymers: (a) 'freely joint' chain model with the delineated Kuhn length (represented in this figure with the *red* straight lines); (b) of the 'warm-like' (Kratky-Porod, KP) model with the exemplified 'curvature' radius, *R*, fitted to a particular (circular) segment of the chain; panels (c) and (d) illustrate key features of the 'comb' (c), and 'bottle-brash' (d) models of branched polymers [1-4,6]. *Black* straight *linear fragments* in the figure (a) represent individual *chemical bonds* (presumably of the (same) bond length, *l*) among neighboring *carbon* atoms within the 'backbone' chain, and with total number of n of such bonds in this particular chain. In the figures (c) and (d) black curves represent 'backbone' chains, while red ones represent 'side' chains (branches).

The Flory's characteristic ratio (FCR), C_n, could be defined based on the mean-square end-to-end distance, $\langle R^2 \rangle$, of a freely joined chain (MW) [1]:

$$\langle R^2 \rangle = C_n n l^2, \tag{1}$$

while its *averaged* (over entire given chain comprising of *n* main-chain bonds of the averaged length *l*), dimensionless C_n, quantity is routinely defined as follows [1]:

$$C_n = \frac{1}{n} \sum_{i=1}^{n} C_i, \tag{1a}$$

with every C_i term being evaluated based on Eq. (1). Flory characteristic ratio, C_n, is related intimately to a *stiffness* of a polymeric chain [1]. For a *perfectly flexible* atomic chain, $C_n \cong 1$ is generally expected based on the Eq. (1a), while for relatively rigid 'double helix' molecules of DNA, the C_n quantity might well exceed 50 [3,4]. The latter definition apparently remains valid both for the *crystalline* and/or *amorphous* linear even branched polymeric chains, though for amorphous molecular structures, inter-atomic distances even within adjacent monomers might be quite close to each other, but not to be exactly same. So-called 'contour length', R_{max}, of the polymeric chain is customarily defined as follows [1]:

$$R_{max} = nl \cos\frac{\varphi}{2}, \tag{2}$$

with the bond angle, φ. A 'backbone' chain comprising merely of *carbon* atoms (which might be bonded differently in general) routinely characterized by the '*tetrahedral* angle', $\varphi \cong 68^o$, between neighboring interatomic bonds [1]. Appropriate combination of the Eqs. (1, 1a, 2) allows one to specify the 'Kuhn length', L_K, of the 'effective' monomer [1-3]:

$$L_K = \frac{C_\infty l^2}{R_{max}}, \tag{3}$$

with the Flory's characteristic ratio, C_∞ , defined via the Eq. (1a) in the $n \to \infty$ limit, or – in other words, – for a case of an *infinitely long* polymeric chain. The L_K length is typically of about 5 to 50 times *longer* than the actual inter-atomic distance (bond length), *l*, in the back-bone chain: $l \cong 1.54$ Å [1]. In fact, the latter (widely accepted) number corresponds to 'single' chemical bond among neighboring carbon atoms in completely equivalent positions, while for such 'double' bond, its length becomes about of 1.34 Å [1-3,17]. Furthermore, bond length among neighboring carbon atoms linked (for instance) to the one and/or two hydrogen atoms would be just of $l \cong 1.50$ Å; these also implies that *angles* among neighboring single and double bonds might 'fluctuate' slightly around the aforementioned 'tetrahedral' one. Just for comparison, length of C=O bond is $l \cong 1.21$ Å, while length of C-O bond is $l \cong 1.45$ Å, length of C-H bond is $l \cong 1.09$ Å [18]. Thus, Kuhn's approximation *replaces* actual backbone chain comprised of n+1 carbon atom with the (average) distance about them equals to *l*, with its 'effective' representation, comprising of N_K 'Kuhn' fragments of the length(s) of L_K each: see also Figure 1(a) for an illustration. The $N_K L_K = R_{max}$ condition is customarily required for the mentioned above Kuhn's parameters of a linear chain [1-3]. This requirement actually allows one to re-write Eqs. (1, 2) above as follows: $N_K L_K^2 = \langle R^2 \rangle$, and $R_{max} = N_K L_K$ (respectively) [1-3]. In other words, transition to the 'Kuhn chain' representation retains some 'global' spatial characteristics of the original polymeric chain, like its 'contour length' and mean-square end-to-end distance. On the other hand, the N_K and L_K parameters of the Kuhn's representation ultimately characterize a 'random walk' behavior of an effective polymeric chain instead of the *n, l,* and C_∞ parameters of a '*rigid*' (up to a certain length of the chain segment) original polymeric chain [1-3].

Another key characteristic of the 'freely rotating' chain is its 'persistence' length, L_p, which characterizes a spatial extent at which local correlations between vectors of inter-carbon atomic bonds vanishing:

$$L_p = \frac{\langle R^2 \rangle}{2R_{max}} = \frac{C_n l}{2\cos\frac{\varphi}{2}}, \tag{4}$$

with the $<R^2>$ and R_{max} parameters defined by Eqs. (1, 2) for a freely rotating chain. Another important characteristic length (scale) of freely rotating model is Flory's length [18]:

$$L_F = l\sqrt{C_\infty}, \tag{5}$$

which is apparently evaluated based on the Flory's characteristic ratio, though in ref [19], a counterpart of the Eq. (5) is used just for *alternative* (as compared to Eq. (3) above) way of definition of the *Kuhn length*, L_K: see Figure 1.49 in ref. [19]. It is noteworthy, that 'Flory length' might be defined as well for very different configurations, with the linear and/or branched polymeric chains, *interacting* among themselves and/or with various solvent(s) [2]. In spite of well-recognized significance of such approximations for generic physics and statistics of polymers, as well as for practical treatments of different polymeric materials, herein we will not discuss them at all, focusing entirely on situation(s) depicting features of interacting and non-interacting linear and branched polymeric chains, presumably 'embedded' into an air (vacuum) environment(s) only.

For such freely rotating (backbone) chains, Flory's characteristic ratio is customarily defined as follows [1]:

$$C_\infty \simeq \frac{1 + \cos\varphi}{1 - \cos\varphi}, \tag{6}$$

and yields $C_\infty \cong 2$ at $\varphi = 68^o$. In contrast, for the 'hindered rotation' model (where dihedral angles among chemical bond are *restricted* by steric interatomic interactions), Flory's characteristic ratio would be expressed in more sophisticated way [3]:

$$C_\infty \simeq \frac{1 + \cos\varphi}{1 - \cos\varphi}\,\frac{1 + \langle\cos\phi\rangle}{1 - \langle\cos\phi\rangle}, \tag{7}$$

with the averaged $<\cos\varphi>$ function of a rotational angle φ. It could be prooved readily, that for freely rotating model, $<\cos\varphi> = 0$ [3]. This condition apparently transforms Eq. (7) to Eq. (6) at the *absence* of correlation(s) among the dihedral angle(s).

So-called '*entropic* spring constant', k_{entp}, of an ideal polymeric chain might be represented by the following equation [1]:

$$k_{entp} = \frac{3k_BT}{N_kL_k^2}, \tag{8}$$

with its dimension, expressed (using SI system) in the $[J/m^2]$ units, while well-known 'mechanical' spring constant is traditionally measured in $[N/m^2]$ units, which are also formally coincides with those of 'stiffness' of solid [20]. Therefore, in order to 'convert' Eq. (8) into the more familiar one, we need to divide its right-hand side by the *l* quantity. In such a case, implementation of the 'corrected' Eq. (8) in combination with the C_∞, N_K, and L_K data, provided in the Table 2.1 of the ref [1], yields $k_{entp} \cong 1.28$ MPa, $k_{entp} \cong 5.17$ MPa, and $k_{entp} \cong 1.19$ MPa at the 'room temperature' ($T_R = 298.15$ K) for the *linear* polyethylene (PE), polypropylene (PP), and atactic polysterene (aPS), respectively. Though those quantities are just about of 5 to 10 times *lower* than the Young modulus of 'high-density PE' (HDPE) eveluated in so-called 'relaxation mode' for their relatively high (40 – 110 °C) temperatures, they are about of 3 orders of magnitude (!) *lower* than of the room-temperature 'tensile' modulus of linear PE, $E_T \cong 400$ GPa, reported by the same authors. In other words, the k_{entp} quantities estimated based on the (corrected) Eq. (8) rather corresponds to mechanical characteristics of *individual* PE chains (MWs), measured at elevated (~90 °C) temperatures, than to the actual mechanical stiffness of entire solid PE [1,21]. It is noteworthy as well, that the entropic 'spring constant' expressed by the Eq. (8) is *temperature-dependent* (i.e., directly *proportional* to the absolute temperature T), which makes its meaning to be quite different from that of ordinary mechanical spring. As it will be shown shortly below in this section, this difference might yield significant consequences for the temperature-dependent lattice thermal capacity of 1D polymeric chains and crystals.

The Hamiltonian, H_{KP}, of the 'Kratky-Porod' (KP) model for an essentially *continuous* 'worm-like' chain reads [2,6]:

$$\frac{H_{KP}}{k_B T} = \frac{\kappa}{2} \int_0^L \left(\frac{d^2 r(t)}{dt^2} \right)^2 dr, \tag{9}$$

with the k_B being Boltzmann's constant, κ is the 'bending stiffness' (expressed in units of energy multiplied by that of length) of the polymeric chain, r(*t*) represent Cartesian coordinate(s) of the chain, while *t* is its 'parametric' coordinate, defined along the contour length R_{max}; see also Figure 1(b) for illustration. Therefore, the 'persistence' length, L_p, could be defined for the KP model using the following ratio [3]:

$$L_p = \frac{\kappa}{k_B T}. \tag{10}$$

In such a case, the counterpart of the Eq. (1) might be expressed as follows [3]:

$$\langle R^2 \rangle = 2L_P \left\{ R_{max} - L_p \left[1 - exp\left(-\frac{R_{max}}{L_P} \right) \right] \right\}. \tag{11}$$

For a sufficiently *long* chain (with $R_{max} >> L_p$), Eq. (11) could be reduced to the following one [3]:

$$\langle R^2 \rangle = 2L_P L. \tag{11a}$$

The free energy, *F*, (expressed herein in *dimensionless* units) of the 'stiff chain' might be composed of the elastic and 'enthalpy' terms, see, for instance, Eq. (7) in ref. [22]:

$$\Delta F = R^2 / \left(L_p R_{max} \right) + v_2 R^2 [(R_{max} / L_P)/R^2]^2, \tag{12}$$

here *R* is the radius of the *appropriate* ('circular', i.e., – with a *constant* radius) *fragment* of the chain (see Figure 1(b) for illustration), v_2 coeffecient chracterizes '…enthalpy due to repulsion…', which is proportional to the '…second virial coefficient…' ($v_2 = L_p^2$) [22]. As it is seen readily from the latter equation, $\Delta F \propto R^2$ (due to its first, and dominant *elastic* term). This implies that the *free energy* of the 'stiff chain' *diverges* in the $R \to \infty$ limit: i.e., when the 'warm-like' chain becomes 'rod-like' one of (formally) *infinite* stiffness. In contrast, the second (enthalpic) term in the latter equation diverges in the $R \to 0$ limit. Thus, though Eq. (12) provides physically meaningful results for idealized 'circular' polymeric chains, it remains valid only within a limited range of variation in its variable argument, *R*.

For a small value of the bond angle, φ, the cosine function in Eqs. (2, 4, 6, 7) might be expanded around unity [1]:

$$cos(\varphi) \simeq 1 - \frac{\varphi^2}{2}. \tag{13}$$

This expansion eventually yields the following (which is an 'alternative' to the Eq. (10)) expression for the 'persistence 'length of KP model:

$$L_p = \frac{2l}{\varphi^2}. \tag{14}$$

Thus, in distinction from the Eq. (10), which defines 'persistence' length of KP model via the 'global' energetic and stiffness parameter(s) of *entire chain*, Eq. (14) expresses this 'persistence' length via purely 'geometrical' (and essentially 'local') quantities characterizing adjacent chemical bonds among backbone carbon atoms. Similarly, expansion depicted by the Eq. (13) allows one to re-define C_∞ and L_K quantities as well [1]. In particular, the C_∞ value might be expressed as:

$$C_\infty \simeq \frac{4}{\varphi^2}, \tag{15}$$

while an appropriate combination of Eqs. (4, 13) eventually yields the following relation for the Kuhn length', L_K [1]:

$$L_K = 2\,L_p. \tag{16}$$

Since both Kuhn and persistence lengths are eventually related to the features of atomic structure of backbone chains of the polymers, in the 'suitable scaling' limit, the freely rotating chain model 'converges' to the 'Kratky-Porod' one of flexible polymers [23,24].

It is worth, however, to be mentioned, that the *idealized concept* of the freely jointed 1D polymeric chain (MWs) is not really appropriate for description of topology of real polymeric materials due to the well-known fact that the *rigid* 'backbone' chains of the *linear, branched* and even those of the *cyclic* polymers cannot cross itself [25]. Instead, fragments of aforementioned backbone chains could rather '… slide-past…' each other, but without crossing [25]. Due to this topological constrain, the *topology* and *movement* of the polymeric chain could hardly be characterized as '…random-walk…' one(s) even at sufficiently large spatial extent (scale). In such a case, 'loop'–type model becomes more appropriate at topological characterization of the real polymeric chain(s). Aforementioned constrain becomes relevant well beyond the 'entanglement' (contour) length, L_e, which customarily exceeds the 'Kuhn length' of the (linear) polymer, L_K, by many (typically more than 10) times [25].

On the other hand, in many cases, bending of a (sufficiently) long 1D polymeric chain would rather emerge in a creation of 3D 'coils', than to formation of 2D 'pattern', sketched, for ins-tance, in the Figure 1(b). Therefore, free energy, Fe, of long continuous polymeric chains usually evaluated based on the volume of a cylinder (tube), which comprises entire 'coil', (for-med with or without embedded 'entangled' segment(s)), see p. 448, Section 25.2 therein [2].

For 'rectangular tubes' inclosing polymeric chain(s) of contour length R_{max}, extension-associated deflection length, λ_{fe}, the *free energy* of confinement, F_{cnf}, could be expressed as follows [26]:

$$F_{cnf}(T) \cong k_B T \frac{R_{max}}{\lambda_{fe}}. \tag{17}$$

For cylindrical 'tubes' of diameter D, $\lambda_{fe} \cong L_p^{1/3} D^{2/3}$ is generally expected, while for the 'rectangular tubes', the λ_{fe} reads [26]:

$$\lambda_{fe} \cong \frac{1}{A_{Od}} L_p^{\frac{1}{3}} \left(L_H^{-\frac{2}{3}} + L_W^{-\frac{2}{3}} \right)^{-1}, \tag{18}$$

with the L_H and L_W quantities are being height and width (respectively) of the rectangular tube [26]. Thus, both for the cylindrical an 'rectangular tubes, the free energy of confinement, F_{cnf}, are expected to be directly *proportional* to the material temperature, T [26].

The $<R^2>$ quantity defined by the Eqs. (1, 11) represents fairly well spatial characteristics of the linear discrete and continuous polymeric chains, while for the *branched* polymers (with multiple 'beginnings' and 'ends' in their molecular structures) this characteristic could be quite meaningless [1]. Instead, so-called 'radius of gyration', $\check{R}_g$, could be introduced in much more meaningful way for branched polymer. The $\check{R}_g$ quantity might be defined as follows [1]:

$$\vec{R}_g^2 = \frac{1}{N_{MP}} \sum_{i=1}^{N} \left(\vec{R}_i - \vec{R}_{cm} \right)^2, \tag{19}$$

with $\check{R}_i$ being an *average* distance between monomers (with N_{MP} being total number of the monomer position vectors) in a given confirmation (spatial configuration), while $\check{R}^{cm}$ is the spatial position of the '*center* of mass' of entire branched chain. The mean-square 'gyration' radius, $\check{R}_g^2$, is well-defined quantity for linear, branched and cyclic monomers: for instance, it equals to just $L^2/12$ for an *ideal linear* chain of the length L, to $N_K L_K^2/6$ for linear 'Kuhn' chains, $N_K L_K^2/12$ for the 'ring' 'Kuhn' polymers, $[(N_K/m)\, L_K^2/6] * (3 - 2/m)$ for m-arm star, and $N_K^2 L_K^2/12$ for rigid 'rod' polymer [1]. An *alternative* (Flory's) approach for evaluation on the $\check{R}_g$ quantity yields [1]:

$$\vec{R}_g \cong L_k N_k^{\nu}, \tag{20}$$

with the 'Flory exponent' of $\nu \cong 0.59$ (or ~3/5) for a 3D chain, while $\nu \cong 3/4$ matches for a chain with 2D topology and $\nu \cong 1$ for 1D one [2].

Though mentioned above in this section morphological, statistical, and mechanical characteristics of linear and branched polymeric macromolecules rather represent they 'classical' (non-quantum) features, they could be linked intimately to their stiffness constants, sound velocities, and even to their key energetic parameters: vibrational (thermal) and even *confinement* energies, spectra, dispersion relations, etc.: see, for instance, Eqs. (8, 17, 18) above in this section. In turn, those key energetic characteristics might be linked unambiguously to the (volumetric) *thermal capacity* of aforementioned individual macromolecules and/or of molecular solids.

On the other hand, so-called 'Tarasov equations' (TEs) are customarily used at quantitative simulations of the temperature-dependent 'harmonic' (i.e., essentially *isochoric*) lattice thermal capacity of linear polymeric chains and their 'layered' counterparts: see for instance, refs. and references therein [10,27,28]. Those TEs were originally created for quantitative descriptions of thermal capacities of chain and layered structures (see also references therein), and widely used for decades at analysis and even predictions of thermal characteristics of various low-dimensional polymeric solids [10,16,27-29]. In particular, implementation of TEs customarily yield $C_v(T) \propto T$, and $C_v(T) \propto T^2$ for the *linear* and *layered* polymeric structures (respectively) at their relatively *low temperatures*; those predictions are apparently significantly deviate from the famous Debye's 'law', $C_v(T) \propto T^3$, established for the similar temperature range(s) of bulk 3D solids [30]. Aforementioned deviations from the 'Debye's law' have to be attributed apparently to the facts that those TEs take into account straightforwardly *diminished* spatial dimensionalities of the chain and layered macro-molecules, and, more specifically, considerable amendments in their vibrational spectra and even in the phonon dispersions, which are modified significantly as compared to their well-known 'bulk' 3D counterpart(s), introduced and discussed in details elsewhere in the prominent work of Peter Debye, dated by 1912! Though key features of TEs are deliberated in details in many well-known publications, they customarily do not incorporate effects of spatial confinement of (non-interacting) acoustic waves and/or thermal atomic vibrations, as well as 'saturation(s)' of the dispersion curves of acoustic phonons (due to effect(s) of so-called 'Periodic Boundary Condition' (PBC)) at their relatively large wavevectors, and – therefore – not able to predict appearance of so-called 'low-temperature anomalies', well-known for the temperature dependencies of the lattice heat capacities of *nano-crystalline* solids, as well as of their low-dimensional counter-parts with limited spatial extension(s). Furthermore, TEs are *not suitable* for description of contribution(s) from anharmonic effects on thermal capacity of those low-dimensional solids [10,16,27-32].

Aforementioned problems were resolved – to some extent – in the seminal works by W. H. Stockmayer and C. E. Hecht, as well as in that by S. M. Genensky and G. F. Newel, published more than 7 decades ago! Their basic approximation(s) presumed existence of vibrational spectrum of 1D *crystals* (comprised with *regularly* arranged MWs) with more *realistic* (as compared to that of the original Debye's model and TEs ones) *phonon dispersion* (which takes into account aforementioned PBC effects, and 'embedded' *interactions* among neighboring MWs: see Figures 2(a), (b) bellow for schematic illustration(s) of those effects. More realistic features of the vibrational spectra of *interacting* MWs eventually yielded significantly amended (as compared to those predicted by the Tarasov's equations) $\mathbf{C_v(T)}$dependencies of their 'molecular crystals': those spectra might become far more complicated as compared to those dependencies, predicted in the ref for the chain molecules [8-10,30-32].

The basic phonon dispersion relation (obtained initially in the ref (see Eq. (2.8) therein), and analyzed and improved further in the refs. [8, 9]), reads :

$$\omega_1^2 = \left(\frac{\alpha}{2}\right)(1 - \cos\varphi_1) + \gamma\,(2 - \cos\varphi_1\,\cos\varphi_2 - \cos\varphi_1\,\cos\varphi_3) + \varkappa\,(1 - \cos\varphi_3)^2\,, \tag{21}$$

where ω_1 stands for the 'circular 'vibrational (phonon) frequency, φ_1, φ_2, and φ_3 are modulus of (normalized) orthogonal vectors (lengths) of the wave number space (i.e., of the phononic Brillouin Zone, BZ); $0 \leq (\varphi_1, \varphi_2, \varphi_3) \leq \pi$. The α quantity in the latter equation is defined by the nearest-neighbor forces; æ related to the forces oppose to the bending of the chain; β is related to the force constant along the chain, while γ is related to the second nearest-neighbor forces; see also Figure 2(b). The following conditions $(\beta/\alpha) > 25$; $(\beta/æ) > 10$, $(æ/\alpha) > 2.5$, and $\gamma \sim \alpha$ are generally expected to be obeyed [8,9].

Moreover, significant simplifications of Eq. (21) could be achieved at the following (a 'qualitative' condition of) $\gamma = \alpha$ [9]. This approximation is based essentially on the consideration that there are strong forces along the chains (Molecular Wires, MWs) and *weaker* ones between them: see Figures 2(a), (b) above for illustration(s). The SH model also incorporates essentially the Born – von-Karman corrections to the original Debye's model with the idealized (i.e., entirely linear) dispersion dependencies of the LA and TA phonons [9,31,32].

In Eqs. (22 – 27) below, the $C_\perp$ symbol refers to *specific heat* contribution from *inter-chain interactions*, while the $C_\parallel$ one to the interactions along the chain; with the 'total 'heat capacity of $C_T = (2C_\perp + C_\parallel)/3$ [9]:

$$C_\perp(T) \propto T^3; \qquad T \ll \frac{\gamma}{2\sqrt{\varkappa}}\, T_m \tag{22}$$

$$C_\perp(T) \propto T^{\frac{5}{2}}; \qquad \frac{\gamma}{4\sqrt{\varkappa}} T_m \leq T \leq \sqrt{\gamma}\, T_m \tag{23}$$

$$C_\perp(T) \propto T^{\frac{3}{2}}; \qquad \sqrt{\gamma}\, T_m \leq T \leq \sqrt{\alpha}\, T_m \tag{24}$$

$$C_\perp(T) \propto T^{\frac{1}{2}}; \qquad \sqrt{\alpha}\, T_m \leq T \leq 2\sqrt{\varkappa}\, T_m \tag{25}$$

$$C_\parallel(T) \propto T^3; \qquad T \ll \sqrt{\gamma}\, T_m \tag{26}$$

$$C_\parallel(T) \propto T; \qquad \sqrt{\alpha}\, T_m \leq T \leq 2\sqrt{\varkappa}\, T_m \tag{27}$$

The T_m quantity in Eqs. (22 – 27) is *proportional* to the *maximum* vibrational frequency, ω_m. Within framework of the canonical Debye's theory, the T_m and ω_m quantities are routinely associated with the Debye's temperature, θ_D, and frequency, ω_D, (respectively) [30].

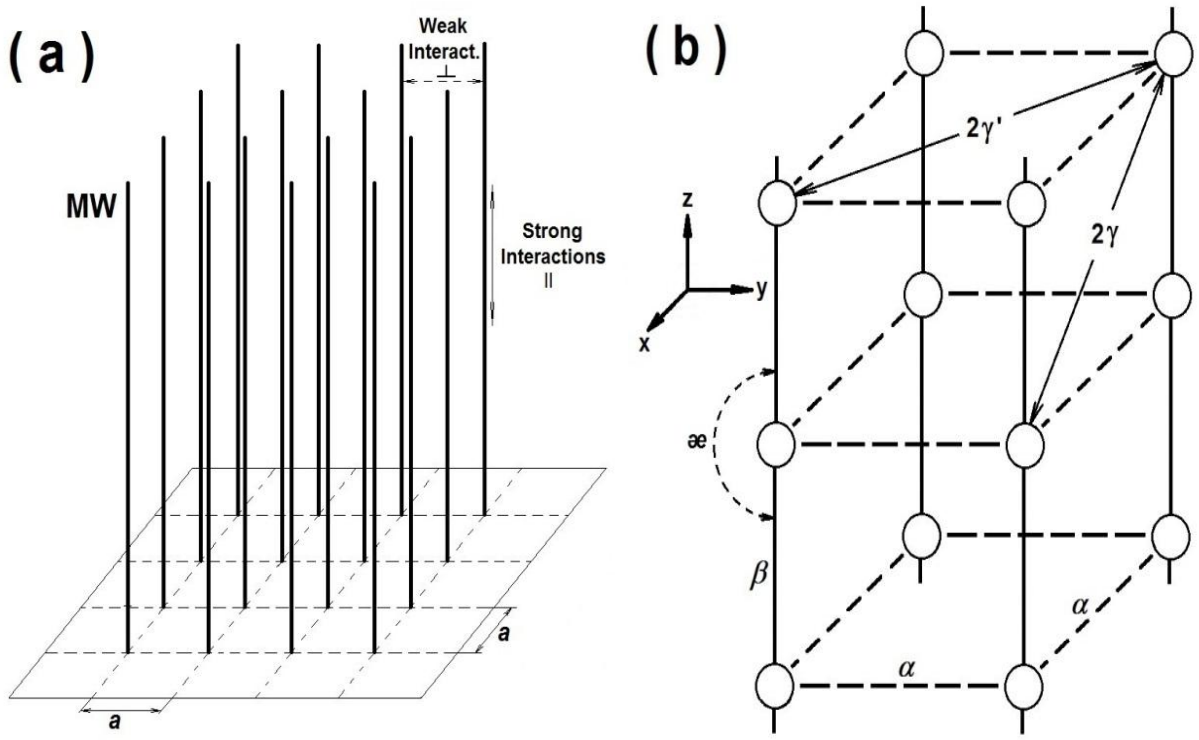

Figures 2(a), (b): 'Macroscopic' (left panel) and 'microscopic' (right panel) sketches of the 'chain (fibrous) polymeric crystal', comprised of *regularly* arranged (i.e., separated by the same 'transverse' distances, **a**) linear *interacting* MWs (solid straight vertical lines in the left panel). Solid straight lines in both panels also represent strong '*longitudinal*', ||, (stretched along the *z* axis in both sketches) interactions within MWs, while dashed lines (curves) in the right panel correspond to (predominantly 'transverse', ⊥, – directed along the x and y axes – and relatively weak) inter-chain interactions. Open circles in the right panel represent 'back-bone' carbon atoms of linear interacting polymeric chains (MWs). The right panel also introduces basic interaction parameters of the model. Both these sketches follow closely to their original counterparts, depicted elsewhere in refs. [8,9]. See also main text for more details.

In other words, the $T_m = \theta_D$, and $\omega_m = \omega_D = k_B\theta_D/\hbar$ equalities (with the 'reduced' Planck's constant, $\hbar$) are presumably hold in such a case. Strictly speaking, the Eq. (24) valids for a 'rectangular' spatial arrangement of MWs (instead of '*squared*' one sketched in the Figure 2(a)); furthermore, the temperature range where Eq. (24) remains valid apparently just *vanishes* at $\gamma = \alpha$. Particular form of the Eq. (27) has to be attributed to the dominant role of the 'strong' '*central forces*', associated with the æ and α constants [9]. This dominance might be formally expressed as follows: $(4æ / \alpha)^{1/2} >> 1$ [9].

In general, the linear $C_v(T)$ enlargement (i.e., $C_v(T) \propto T$) with the temperature (predicted by the Eq. (27)) is expected for linear (1D) polymeric chains (MWs): see, for instance, discussion on this issue in the introductory part of ref. [16], as well as references therein. In contrast, the $C_\perp(T) \propto T^\eta$ behavior is typical for the 'bulk' 3D semiconductors and insulators; see also Eqs. (22, 26) above. It is noteworthy, that 'transverse' inter-chain (MWs) interactions routinely yield $C_\perp(T) \propto T^\eta$ dependencies with the 'fractional' exponent, η, of 0.5, 1.5, and of 2.5 in the Eqs. (25, 24, 23) respectively [16,30].

Similar behavior, $C_v(T) \propto T^D$, might also emerge for *brunched* polymers with the 'fractal' structural dimensionality, D, and topology of their atomic structure(s) [33-35]. Amendment in the lattice topology and in its fractal, dimensionality might have quite direct impact on the statistical and mechanical parameters of those low-dimensional polymers. For instance, Flory's characteristic ratio, C_∞, for branched polymers, might be expressed as follows [33]:

$$C_\infty = \frac{\mathfrak{D}}{3\,(2-\mathfrak{D})} + \frac{4}{3}\,, \tag{28}$$

with the (fractal) dimensionality of the polymer, *D*. The latter equations differ significantly from its counterparts, expressed by the Eqs. (1a, 6, 7). For the well-distinguished fractal structures, like 2D-based Sierpinski fractal 'carpet' and 3D-based Sierpinski 'sponge', their fractal dimensionalities equal to $D(2) \cong 1.89278$, and to $D(3) \cong 2.72683$, which (based on the Eq. (28)) yield $C_\infty = 7.218$ for the 2D-based case. For the 3D-based case, denominator of the first term in the Eq. (28) apparently becomes negative; thus, implementation of this entire equation for the 3D-based case becomes questionable. Just for comparison, $C_\infty = 7.4$, $C_\infty = 5.9$, and $C_\infty = 9.5$ are tabulated for the polyethylene, poly-propylene, and atactic poly-styrene (respectively) in the Table 2.1 of the refs. [1,35]. In other words, appropriate 'fractal' counterparts (at least developed for the 2D-based case) of the well-known 'canonical' equations for structural characterization and rigidity of some linear and branched polymers might yield fairly reasonable approximation(s) for their well-established parameters based on very generic topological considerations. On the other hand, based on the 'fractal dimensionality' model, $C_v(T) \propto T^{1.89278}$ is expected for 2D-based Sierpinski 'carpet' and $C_v(T) \propto T^{2.72683}$ for the Sierpinski 'sponge', which does not really match to the features(s) experimental temperature-dependent lattice thermal capacity of real polymers [16]. Those discrepancies have to be attributed to essentially 'artificial' structural (topological) features of the Sierpinski's 'carpet' and 'sponge', which do not depict many actual features of real polymeric topology.

Therefore, other structural and topological models of polymeric macromolecules are discussed widely for decades [36]. Based on the classification provided elsewhere in the, *branched* polymers could be specified as '*ridge-like*' (with their branches connected to the main ridge), statistical (comprised of macromolecules without main ridge), and *star-shaped* (with all branches linked to the one 'origin') [36]. Nevertheless, for any type of branching, the number of branches p_B of the given macromolecule is defined by its number of nodes b and the 'functionality' of the branch's f_B [36]:

$$p_B = (f_B - 1)\, b + 1. \tag{29}$$

Then, the branching density ρ_B equals to the ratio: $\rho_B = (\alpha_B * b) / x_B$, with degree of polymerization x_B, while α_B being a constant depending on it [36].

Yet another fairly simple model of the *branched* ('cross-linked') polymer presumes existing of molecular 'linkages' (bridges) among neighboring linear macromolecules [21]. In such a case, 1D macromolecular structure(s) apparently becomes 3D one(s) in general, and it allows one to define meaningfully not only their 'longitudinal' elastic constant (modulus), the only distinct one for those 1D structures (see, for instance, Eq. (8) above), but also 'shear' (transverse) one, G_0, which is well-established predominantly for 3D solids, and reads [21]:

$$G_0 = \frac{\rho\, R_0\, T}{M_c}, \tag{30}$$

with the *mass density* of solid polymer, ρ, the R_0 is 'universal gas constant', and M_c is the molecular weight of (predominantly) *linear fragments* of macromolecules, stretched between those cross-links (bridges). The latter equation is often used at the quantitative evaluations on the molecular masses of various cross-linked (branched) polymers based on their experimentally obtained shear modulus G_0 [21]. It is noteworthy, that – in spite of the significant differences in the physical essences of the 'linear' spring constant, defined by the Eq. (8), and the 'bulk' shear modulus, defined by the Eq. (30) – both these quantities are increasing *linearly* with the enlargement in absolute temperature, T. More sophisticated models (concepts) of the network topology of branched polymers might be developed as well based on the graphs theory, Bethe lattice approximation, random chain configuration(s) (with the self-avoiding constraint), using so-called 'dendrimers', and 'hyper-branched' models of polymers, percolation approach, etc. [2].

For a 'hyper-branched' (HB) polymers, containing 'Dendric' (D), 'Terminal' (T), 'Linear' (L) and 'Initial' (I) structural units, so-called 'Degree of Branching', DB, reads [37]:

$$DB = \frac{D + T}{D + T + L}. \tag{31}$$

This DB index equals to zero, for simple purely *linear* polymeric chains, while it is approaching unity for the 'hyper-branched' polymers composed mainly of the 'Dendric' and 'Terminal' units. Thus, in contrast to the p_B quantity, defined by the Eq. (29), the DB index expressed by the Eq. (31) yields a 'normalized' number of branches.

One of the mostly reconnoitered modifications of the HB polymers is so-called 'bottle-brush' macromolecules; see also references therein and Figure 1(d) above for an illustration [38]. This particular modification of HB polymers might form '…stiff, cylindrical, and shape-persistent structures…' [38]. Furthermore, 'High branching densities can lead to strong stiffening of the backbone due to steric overcrowding of the side chains in the densely packed brush'. As a result, the Kuhn length, L_K, of such bottle-brush structure(s), evaluated *experimentally* via dynamic- and static-light scattering techniques, might be as high as 70 ± 4 nm, which exceeds by many (~46) times its counterpart evaluated for the '...bare backbone…' of the poly (alkyl methacrylate), PAM [38]. Fractal dimensionality of the 'brush' is estimated to be of $D = 1.64 \pm 0.08$, which is quite close to that '…expected for a *three-dimensional* (?) self-avoiding random walk…' [38].

Amendments in the molecular structures and topology of many well-known polymeric solids might also affect considerably their *vibrational* and *thermal* characteristics, though experimental temperature dependencies of their lattice thermal capacities often exhibit 'tenacious' common features, which emerge importunately regardless to the chemical, structural and topological features of those macromolecules, see sub-section 2.2 below for details. In order to discuss persuasively contributions of various chemical, structural and topological factors to the particularities of the temperature-dependent lattice thermal capacities of different types of solid polymers comprised of (predominantly) linear and branched macromolecules, we have to comprehend briefly their chemical composition(s) and structural features. Those features are illustrated and discussed briefly in the *next* sub-section.

2.2. Molecular Features of Some Low-Dimensional Solid Polymers

Molecular structures of some well-known 'industrial' linear and branched polymers usually comprised of 'back-bone' chain(s) of interlinked carbon atoms, 'complemented' with isolated 'peripheral' hydrogen atoms, and/or 'terminal' structural groups, composed of the carbon and hydrogen atoms only [1-3]. More sophisticated polymeric structures might comprise of 'cyclic' components, like 'aromatic rings', (e.g., benzene, pyridine, pyridinium, cyclopentadienyl, and cyclo-heptatrienyl ones), as well as biphenyl, naphthalene, pyrol, pyrrole, thiophene, and indene molecular rings, alongside with the (isolated) nitrogen, oxygen, sulfur (etc.) atoms, which might be incorporated both into 'backbone' polymeric chains, and/or into different types of 'terminal' groups and cyclic structures as well [1-3].

Chemical (atomic) composition(s) of molecular units (monomers) and sketched structures of macro-molecules of some well-known *linear* solid polymers are specified in the Table 1. Those linear polymeric chains are comprised of (predominantly) *carbon* backbone atoms only alongside with the 'isolated' hydrogen, fluorine, and chlorine 'terminal' atoms. However, repetitive *alteration* of the *single* and *double* chemical bonds among neighboring carbon atoms might occur for backbones of linear MWs based on relatively long monomers, like poly-butadiene (PBDN). On the other hand, the 'backbone' chains of the MWs of polyglycine (PGCN) and polyurethane (PU) incorporates *oxygen* and *nitrogen* atoms as well, see two bottom rows of the Table 1. The oxygen and nitrogen atoms might also be attached as the 'terminal' ones to the backbones PGCN and PU macromolecules.

In the Table 1, the *MolView* (version 2.4) software is used at creation of graphical representations of the structural units of all linear *monomers*, while ChemSketch (freeware), version 2.4 (2023), is used for creating of sketches of atomic arrangements within all those linear polymeric structural units. The grey, green, light green, blue and red balls represents carbon, chlorine, fluorine, nitrogen, and oxygen atoms (respectively), while white ones represent hydrogen atoms in the graphical illustrations of monomers.

The Table 2 reveals molecular structures of some well-known 'branched' polymers and their monomers, with the 'separated' CH_3 (methyl), CO (carbonyl), NH_2 (amino), and CN (cyano) terminal groups, and/or combination(s) of those terminal groups. Again, the MolView (version 2.4) software is used at creation of graphical representations of the structural units of all linear monomers, while ChemSketch (freeware), version 2.4 (2023), is used for creating of sketches of atomic arrangements within all those linear polymeric structural units. The grey, green, light green, blue and red balls represents carbon, chlorine, fluorine, nitrogen, and oxygen atoms (respectively), while white ones represent hydrogen atoms in the graphical illustrations of monomers.

It is noteworthy, that the V_{mnm} abbreviation in the head of the 4th column of this table (as well as in the other tables shown below in this sub-section) represents so-called '*monomer volume*' (tabulated, for instance, for some polymers in the Table 19.2 of the ref. [2], while N_{AT}^{mnm} in the head of the fifth column stands for the total *number* of *atoms* of the given *monomer*. For polymers not reflected in that Table 19.2, the Vmnm quantity is evaluated based on the following (generic) relation: $V_{mnm} = 1.66 \times 10^{-3} * M_M / \rho_M$, with the M_M being *molar mass* of the monomer expressed in the (g/mol) units, while ρ_M stands for its mass density (g/cm^3); see also comments to the Table 19.2 of the ref. [2]. Those evaluated Vmnm quantities tabulated in the fourth column of the Tables 1-4 are marked oud with the 'star' symbol.

Macromolecule	Notation	Monomer Structure	V_{mnm}, nm^3	N_{AT}^{mnm}	Polymer Outline
Polyethylene	**PE**	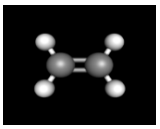	0.119	6	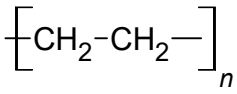
PolyVinyl-Chlorid	**PVC**	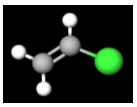	0.078*	6	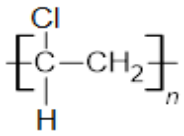
PolyVinyl-Fluorid	**PVF**	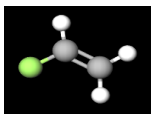	0.053*	6	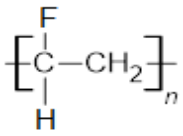
PolyTetraFluro-Ethylene	**PTFE**	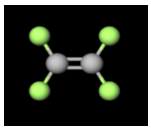	0.079*	6	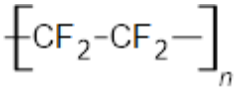
Poly(chlorotri-fluorethylene)	**PCTFE**	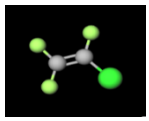	0.091*	6	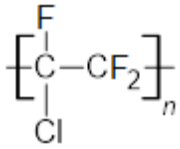
Poly(butadiene) (1,4)	**PBDN**	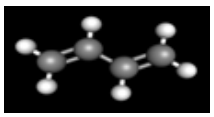	0.108*	10	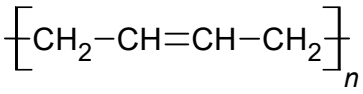
PolyGlycine	**PGCN**	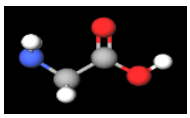	0.062*	7	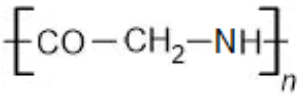
PolyUrethane	**PU**		0.324*	11	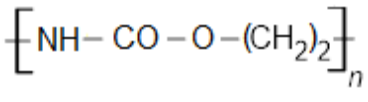

Table 1: Molecular Structures of Some Linear Polymers

The Table 3 summarizes basic structural features of some *cyclic* monomers and their macro-molecules, while the Table 4 exhibits similar structural features of two simplest *aminoacids*.

Macromolecule	Notation	Monomer Structure [a)]	V_{mnm}, nm^3	N_{AT}^{mnm}	Polymer Outline
PolyAcryloNitrile	**PAN**		0.069*	7	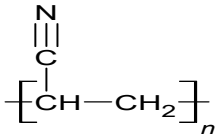
Polypropylene	**PP**	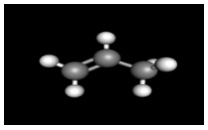	0.176	9	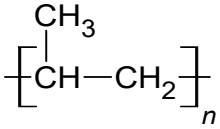
Polyisoprene	**PIP**	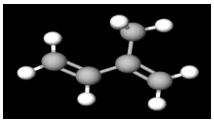	0.113*	13	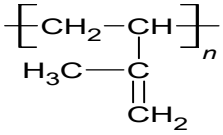
PolyMethaCrilic Acid	**PMAA**	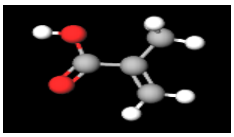	0.119*	12	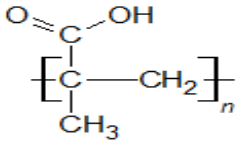
PolyMethylAcrylate	**PMA**	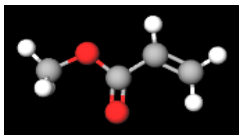	0.143*	12	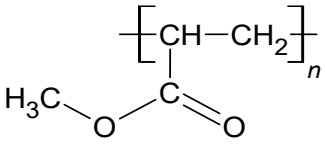
PolyMethylMetha-Crylate	**PMMC**	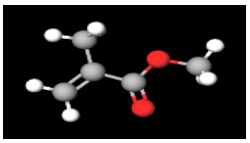	0.149	15	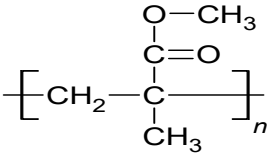
PolyMethaCrylAmid	**PMAM**	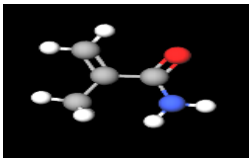	0.119*	13	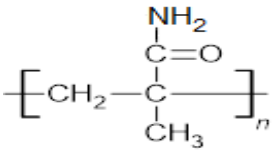

Table 2: Molecular Structures of Some Well-Known Branched Polymers

Macromolecule	Notation	Monomer Structure	V_{mnm}, nm^3	N_{AT}^{mnm}	Polymer Outline
PolyStyrene	**PS**	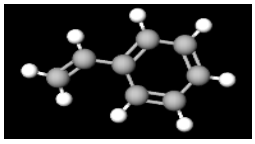	0.179	16	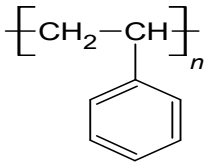
PolyAlphaMethyl-Styrene	**PαMS**	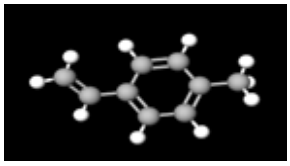	0.185	20	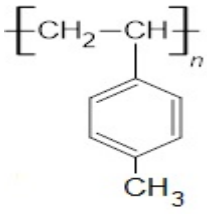
PolyEthylene-Terephtalate	**PET F**	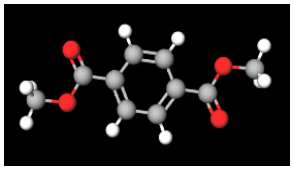	0.266*	22	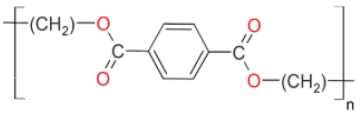
Polyglycolide	**PGL**	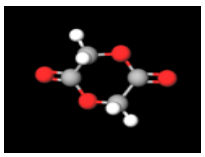	0.058*	6	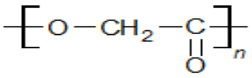
PolyCapro-Lactone	**PCL**	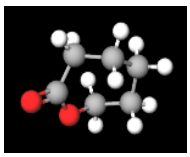	0.165*	18	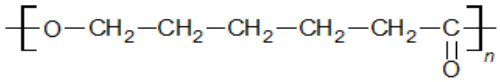

Table 3: Molecular Structures of Some Well-Known *Cyclic* Polymers

The MolView (version 2.4) software is used at creation of graphical representations of the structural units of all linear *monomers*, while ChemSketch (freeware), version 2.4 (2023), is used for creating of sketches of atomic arrangements within all those linear *polymeric* structural units. The grey, green, light green, blue and red balls represents carbon, chlorine, fluorine, nitrogen, and oxygen atoms (respectively), while white ones represent hydrogen atoms in the graphical illustrations of monomers.

Macromolecule	Abbreviation	Monomer Structure [a)]	V_{mnm}, nm^3	N_{AT}^{mnm}	Polymer Outline
Poly L-alanine Alpha	**PLAA**	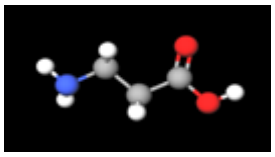	0.091*	10	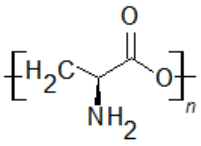
Poly L-Valine	**PLV**	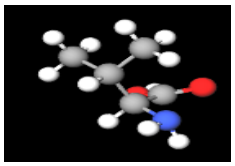	0.158	16	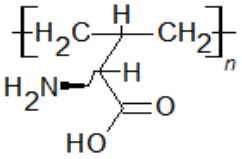

Table 4: Molecular Structures of Two Simplest Aminoacids

In general, the 'electronegativity' of aforementioned oxygen and nitrogen atoms deviate significantly from those of carbon and hydrogen atoms, and such differences eventually yield additional dynamic Coulomb (i.e., predominantly dipole-dipole – due to iconicity of the C-H, C-O and/or C-N, N-H chemical bonds) interactions among different fragments of the same polymeric chains, as well as among neighboring such chains; see alsoFigures 2(a) and 2(b) above for an illustration. As it will be discussed briefly in the next sub-section, those additional (Coulombian in their nature) dynamic interactions might contribute significantly to the vibrational and energetic characteristics of such macromolecules and eventually affect significantly features of the temperature dependencies of lattice heat capacity of those particular macromolecules, especially for those mentioned in the Table 4 above [39]. It is noteworthy, that cyclic (ring) topology of the PGL and PCL emerges only for their mono-molecular (monomeric) structures, while their macromolecules rather exhibit relatively simple linear atomic arrangements with alternating hydrogen and oxygen terminal atoms of the essentially 1D backbone chain(s) with both carbon and oxygen atoms embedded into their atomic structures, in an apparent similarities with the backbones of the liner PGCN and PU, shown in the Table 1: see two last rows in the Table 3 for illustration(s). On the other hand, structures of macromolecules of the PLAA and PLV rather correspond to those of branched polymers, with both carbon and oxygen atoms incorporated into their backbone(s) as well, and relatively complex (especially in the case of PLV) atomic structures of their branches: see Table 4. Nevertheless, – in general – essentially different chemical (atomic) composition(s) of monomers and topologies of macromolecules of the well-known linear (listed in the Table 1), branches (Table 2), and cyclic (Table 3) polymers, as well as those of simplest aminoacids (Table 4), might eventually yield unique features in their temperature dependencies of isobaric lattice thermal capacities, $C_p(T)$. The next sub-section is devoted to description of those experimentally evaluated $C_p(T)$ dependencies and very brief discussion on the relation-ships among their features and structural particularities of aforementioned macromolecules.

2.3. Temperature-Dependent Lattice Thermal Capacity

Intensive experimental and theoretical investigations on the characteristics of thermal capacity of polymers emerged as an important branch of material science and engineering soon after the end of the World War II (see also references therein). Later, those studies were also 'expanded' to the medical and biological sciences [10,16,40-44]. Below in this sub-section, typical temperature dependencies of the lattice thermal capacities of some typical linear, brunched, and cyclic polymers, as well as those of simplest aminoacids are plotted based on the data, tabulated elsewhere in refs. [45-48]. In particular, Figures 3(a), (b), reveal the $C_p(T)$ dependencies, plotted based on the data, tabulated else-where in the refs. for the linear amorphous poly-Ethylene, polyTetra-FluroEthylene, crystalline polyChloroTri-FluorEthylene, polyVinylChloride, polyVinylFluorid, poly(butadiene) (1,4), polyGlycine, and 'glassy' polyUrethane. As it is seen from the Figures 3(a), (b), all plotted experimental $C_p(T)$ dependencies exhibit close to linear (i.e., with the log-log slopes ranging from ~0.7 to ~1.0) enlargement with the tem-perature at elevated temperatures (typically exceeding 50 – 100 K), alongside with relatively sharp $C_p(T)$ decline with the temperature diminishment at relatively low temperatures [45-48]. Those distinct declines in $C_p(T)$ dependencies are customarily denoted as 'low-temperature anomalies': see, for instance, and references therein. Nonetheless, every plotted $C_p(T)$ curve could be approximated reasonably well (though within limited temperature ranges) with cubical polynomials, represented, for illustration purpose(es) with the dashed curves in Figures 3(a), (b) [16,17].

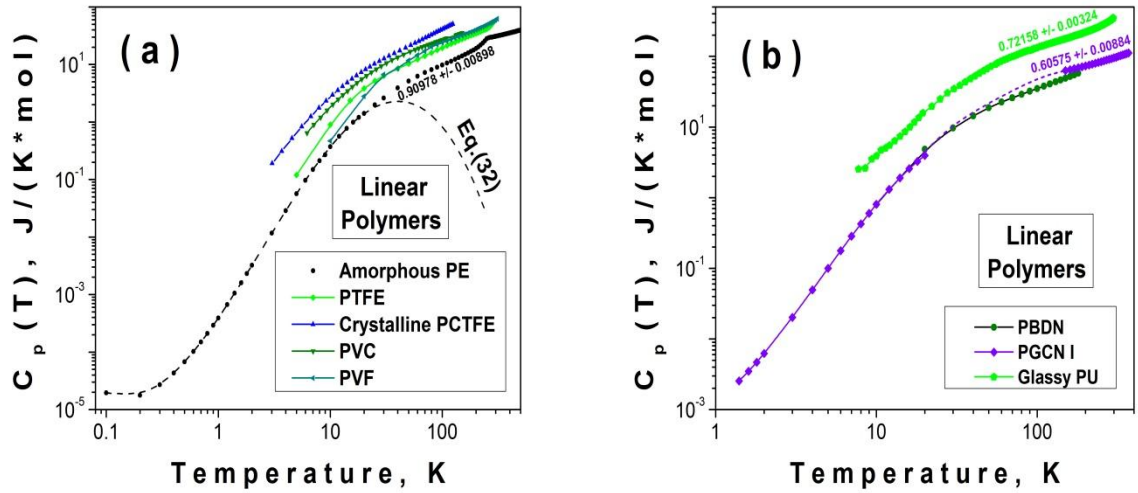

Figures 3(a), (b): (color online). Experimental (filled symbols connected with the straight lines for eye guide) temperature-dependent lattice thermal capacity of several linear polymeric macromolecules, plotted based on the 'recommended' data, tabulated elsewhere in the refs: see, in particular, Tables 3, 4, and 5 in ref, as well as Tables 21, 25, 28, 31, 33, 35 in ref, [46]., and Table 17 in ref. [45], alongside with the Table 17 in ref. [46], 18 in the ref, and Table 1 of refs. [45-48]. The log-log slope(s) of the experimental $C_p(T)$ dependencies are evaluated within the temperature range of (20 K ≤ T ≤ 200 K) using standard least-square-fit procedure(s) for amorphous PE in the panel (a) as well as for the gassy PU (green figures) and PGN (blue figures) in the panel (b), and indicated in the close vicinity of appropriate curve. Dashed curve in panel (a) represent polynomial approximations; see main text for details. This curve corresponds to the Eq. (7) ref. [45].

For the case of linear PE, the appropriate polynomial approximation is expressed by the Eq. (7) in the ref. (which is expected to be valid for the temperature range 0.5 K ≤ T ≤ 20 K), and *re-numerated* as Eq. (32) below. The latter equation reads:

$$C_p(T) = exp[-0.135328\ (\ln T)^3 + 0.363949\ (\ln T)^2 + 2.85597\ (\ln T) - 7.84553]\ , \qquad (32)$$

see also Eq. (7) in ref. [45].

Similarly, other experimental $C_p(T)$ dependencies, tabulated elsewhere in refs for the linear PVC, PVF, PTFE, PCTFE, and PGCN, and plotted herein in the Figures 3(a), (b), could be approximated (though within certain temperature ranges) with appropriate cubical polynomials. However, those polynomial approximations are *not revealed* in the latter figures [46,47].

The Figure 4 shows experimental $C_p(T)$ dependencies, plotted for few well-known *branched* polymers, based on the data tabulated elsewhere in refs. [47,49]. Similar to the $C_p(T)$ curves plotted in the Figures 3(a), (b), their counterparts plotted in the Figure 4 exhibit *sub-linear,* and (almost) linear sub-ranges at elevated temperatures, as well as well articulated 'low-temperature anomalies'. Furthermore, all experimental $C_p(T)$ dependencies, shown in the Figure 4, might be approximated as well with 'cubical' polynomials (though within limited temperature ranges). Particular examples of two such polynomials are plotted in the latter figure with dashed curves. For poly-2-methylbutadiene – or polyisoprene (PIP), the following polynominal equation is used (at approximation of experimenta data) on the page 42 of the ref. [46]:

$$C_p(T) = exp[0.0116251\ (\ln T)^3 - 0.603157\ (\ln T)^2 + 4.6949\ (\ln T) - 6.88471]\ , \qquad (33)$$

which is expected to be valid within the temperature range of (2.5 K ≤ T ≤ 10.6 K).
As for the case of *branched* Poly-MethylAcrylic-Acid (PMAA) – see the forth line in the Table 2 –, the appropriate polynomial approximation is expressed by the Equation (X) in the Table 25 in the (which is expected to be valid within the temperature range of 10 K ≤ T ≤ 279 K), and re-numerated as Eq. (34) herein [49]:

$$C_p(T) = exp[0.0566117\ (\ln T)^3 - 0.929753\ (\ln T)^2 + 5.88628\ (\ln T) - 9.10792]\ . \qquad (34)$$

Similarly, for the (*branched*) crystalline PP, the following *cubical* polynominal is used at approximation of experimental data tabulated elsewhere in the Table 4 of the ref. [50]:

$$C_p(T) = exp[-0.130693\ (\ln T)^3 + 0.249189\ (\ln T)^2 + 0.0816695(lnT) + 5.41896]\ . \qquad (35)$$

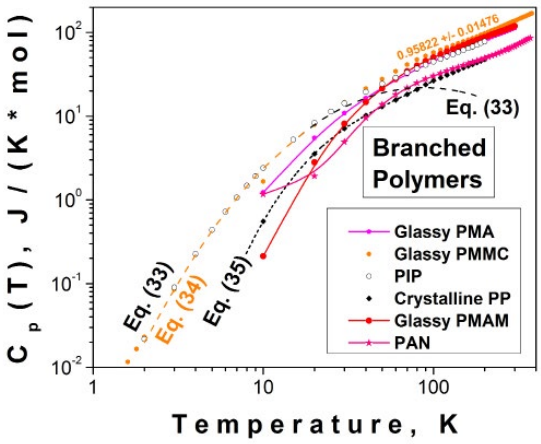

Figure 4: (color online). Experimental (filled symbols connected with the straight lines for eye guide) temperature-dependent lattice thermal capacity of several *branched* polymeric macro-molecules, plotted based on the 'recommended' data, tabulated elsewhere in the Tables 4, 6, 22 of the ref. [49] and Table 6 of the ref. [50], respectively. Log-log slope(s) of the plotted experimental $C_p(T)$ dependencies are evaluated using standard least-square-fit procedure(s) for amorphous PMMC, and indicated in the close vicinity of appropriate curve. Dashed curves in both panels represent *cubical* polynomial approximations of the experimental data; see Table 2 for polymer abbreviation, and main text for more details [49,50].

As it is seen from the Figures 3(a), (b), and 4, all aforementioned polynomial approximations *deviate* significantly from their experimental counterparts beyond their *designated* temperature ranges. The Figure 5 reveals experimental $C_p(T)$ dependencies, plotted based on the data, tabulated in for 5 cyclic polymers. Again, all $C_p(T)$ dependencies plotted in the latter figure exhibit sub-linear and (almost) *linear* enlargements with the temperature at elevated temperatures (exceeding ~ 100 K), as well as the 'low-temperature anomalies' below that temperature range [45,47].

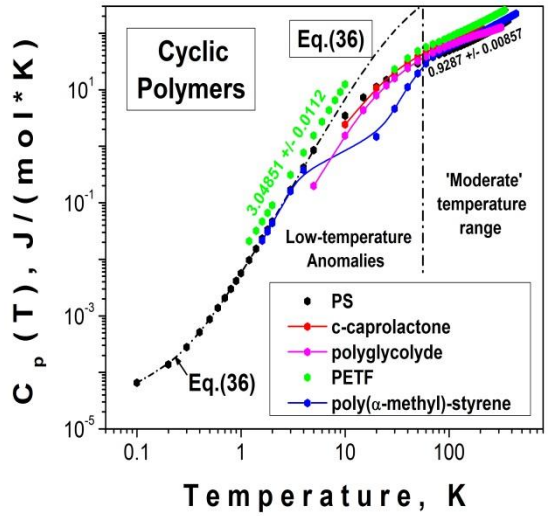

Figure 5: (color online). Experimental (filled symbols connected with the straight lines for eye guide) temperature-dependent lattice thermal capacity of several cyclic polymeric macro-molecules, plotted based on the 'recommended' data, tabulated in Tables 4, 7, 10 elsewhere in the refs. [47,51]. Log-log slope of the plotted experimental $C_p(T)$ dependence is evaluated within the temperature range of (80 K ≤ T ≤ 300 K) using standard least-square-fit procedure(s) for the case of PS, while for the PETF this slope is evaluated within the (2 K ≤ T ≤ 20 K) range. Dashed curve represents *polynomial* approximations of the (relatively low-temperature) experimental data reported for the PS based on the Eq. (36) in main text.

Furthermore, the following cubical polynomial approximation matches for the case of PS [51]:

$$C_p(T) = exp[-0.0738699\ (\ln T)^3 + \ 0.25189\ (\ln T)^2 + 2.90478\ (\ln T)\ - 5.21616]\ , \qquad (36)$$

which was fitted to the experimental data for the absolute temperatures below 5 K; see also Eq. (3) in the; p.321 therein. As it is seen from the Figure 5, the polynomial approximation deviates significantly from the experimental data plotted for the PS for the temperatures well exceeding 5 K [51].

The Figure 6 reveals temperature dependencies of the lattice heat capacities of poly-L-valine, and poly-L-alanine alpha, plotted based on the 'recommended' data, tabulated elsewhere in the ref. [47]. Both $\mathbf{C_p(T)}$ dependencies enlarge 'super-linearly' (with the log-log scale of ~1.33 and ~1.70) with the temperature increment above T ≅ 20 K, but decline quite rapidly with the temperature diminishment at relatively low temperatures, see Figure 6.

It is noteworthy, that the following polynomial approximations was fitted to the $C_p(T)$ dependence, 'recommended' for the poly-L-alanine-alpha, and plotted in the latter figure:

$$C_p(T) = exp[-0.0434849\ (\ln T)^3 -\ 0.0728239\ (\ln T)^2 + 3.09478\ (\ln T)\ - 3.11191]\ , \qquad (37)$$

within the following temperature range: 1.5 K ≤ T ≤ 10 K; see also Table 19 in the ref. [51].

Thus, as a (brief) summary to this sub-section, *all* experimental (or 'recommended') $C_p(T)$ dependencies tabulated elsewhere in, and for the *linear*, *branched*, and *cyclic* polymers, as well as for simplest amino-acids, and plotted herein in the Figures 3(a), (b), 4, 5, and 6 (respectively), exhibit key *common* features. In particular, at *elevated* temperature (typically exceeding 20 K – 50 K), those experimental $C_p(T)$ dependencies reveal *sub-linear* (in Figures 3(a), 3(b), 5), (almost) linear (in Figure 4), and 'super-linear' (in the Figure 6) enlargement(s) with the temperature, alongside with clearly articulated 'low-temperature anomalies' in all plotted $C_p(T)$ herein dependencies at relatively low temperatures [19,44,48,51]. Those 'anomalies' are manifested in relatively sharp and essentially non-linear $C_p(T)$ decline(s) with the temperature diminishment. Aforementioned archetypal $C_p(T)$ features are replicated reasonably well within certain temperature range(s) with the (appropriate) *cubical polynomials* (see *dashed* curves in all figures plotted in this sub-section), though *withought* any *reference* to (even hypothetical) *physical origins* behind such archetypal behavior.

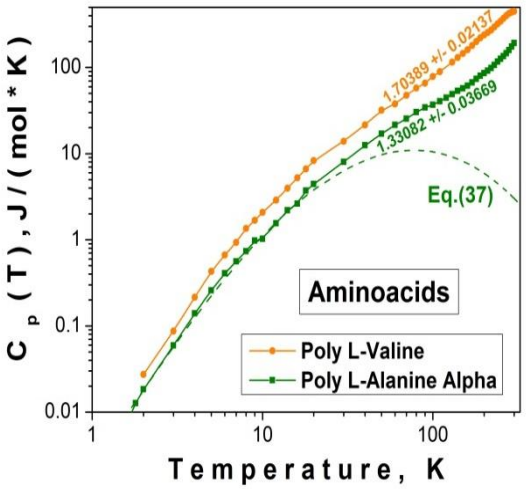

Figure 6: (color online). Experimental (filled symbols connected with the straight lines just for eye guide) temperature-dependent lattice thermal capacity of poly-L-valine, and poly-L-alanine alpha, plotted based on the 'recommended' data, tabulated elsewhere in the Tables 21 and 24 of the ref. [47]. Log-log slope(s) of the plotted experimental $C_p(T)$ dependencies are evaluated within the temperature range of (20 K ≤ T ≤ 200 K) using standard least-square-fit procedure(s), and indicated in the close vicinity of appropriate curve. Dashed curve represents polynomial approximations of plotted the experimental $C_p(T)$ data for poly-L-alanine-alpha, expressed by the Eq. (37); see main text for more details.

The next section of this article is devoted to the discussion on thinkable physical reasons causing the depicted above $C_p(T)$ behavior for linear, branched and cyclic polymers, as well as resounding approximation(s) on the aforementioned $C_p(T)$ dependencies based on (primarily one-dimensional) 'spatial confinement' and molecular rotation(s) phenomena, as well as to the appropriate discussion of all obtained simulation results in comparison with prediction(s) of well-known structural and topological models of low-dimensional polymeric materials, discussed in the *sub-section* 2.1 above, and results of independent experimental evaluations.

3. Simulation Approaches and Results

3.1. Simulation Formalism

As it will be shown shortly below in this section, the $C_p(T)$ dependencies plotted in the sub-section 2.3 might be replicated and interpreted reasonably well based on the (appropriately *re-normalized*) *one-dimensional* (1D) basic equation of so-called 'Generalized Skettrup Model' (GSM), with its original form provider elsewhere in the, see also references therein [16]:

$$C_p^{1DGSM}(T) = \frac{C_1}{k_B T^2} \sum_{N=1}^{N_M} \sum_{p=1}^{N\, p_{max}} \frac{exp\left(p\frac{E_{min}}{k_B T}\right)}{\left[exp\left(\frac{p\, E_{min}}{k_B T}\right) - 1\right]^2} \frac{(p\ E_{min})^2}{N!\ (Z_{1D}^N)} \left[floor\left(\frac{L_z}{a_l\, N}\right)\right]^N, \qquad (38)$$

here C_1 is the *dimensional* 'normalizing coefficient', the function *floor*(*x*) returns an integer part of its *rational* argument, a_l is an (average) *interatomic* distance ('lattice constant') of the MW material, k_B is the Boltzmann constant, E_{min} is the 'minimal' energy of the phonons, confined within 1D polymeric MW, $Z_{1D}{}^N$ is the N-particle 'statistical sum' (N-phonon partition function), while c_{eff} is an *effective* sound velocity, routinely defined as follows: $3/c_{eff} = (1/c_l + 1/c_{t1} + 1/c_{t2})$, where c_l stands for the *longitudinal* sound velocity, while c_{t1} and c_{t2} denote two (different in general) transverse sound velocities of the MW material [16].

In general, the specific (algebraic) expression and the *dimension* (physical units) of the ref. [2]. C_1 coefficient might be defined in several different ways. Probably the most physically meaningful and straightforward way entails the C_1 definition as the (volumetric) *atomic density*, ρ_{AT}, of the 1D chain: $C_1 = \rho_{AT} = N_{AT} / V_0$, with the N_{AT} being the number of atoms in its repetitive molecular fragment, and V_0 is the volume of such fragment. This C_1 definition brings in naturally the *energy-independent* (as generally expected) 1D *Density-Ofatomic-States* (DOS), into the right-hand side of the latter equation. Actually, the DOS terms are quite common for many equations created for simulations on the temperature-dependent thermal capacity of a solid; see also references therein, and – in our particular case

– makes the dimension of the entire $C_p^{1DGSM}(T)$ term defined by the Eq. (38) to be equal to the [J / (K * cm^3)], i.e., it eventually simply turns to be the *volumetric* thermal capacity of the 1D semiconductors and insulators [16,30]. This definition is apparently suitable not only for the linear and branched polymeric chains, but actually for any 1D chain predominantly linked via the covalent and/or ionic inter-atomic bonds, either with a strictly *periodic* (crystalline) atomic arrangement(s), or even for those chains with the spatially disordered (amorphous) atomic arrangements. At the same time, such definition of the C_1 coefficient is directly applicable to the low-dimensional polymeric materials, mentioned – for instance – in the sub-section 2.2 of this article. Indeed, in the latter cases, the ρ_{AT} and C_1 quantities of the given polymeric material could be subtracted directly from the fourth and fifth columns of the Tables 1 – 4, as the appropriate ratio(s) of the N_{AT}^{mnm} / V_{mnm} parameters, listed in those columns of the aforementioned tables. More generic way of definition of the ρ_{AT} quantity might be based on the following algebraic expression: $\rho_{AT} = \rho_M N_A N_{AT} / W_{mol}$, with the *mass* density of the polymeric material, ρ_M, and the Avogadro's number, N_A, while the W_{mol} stands for the molecular weight of the 1D material (polymeric chain). In such a case, the physical meaning of the C_1 quantity still could be identified with the DOS one [52].

Alternatively, the C_1 coefficint might be defined as follows: $C_1 = N_{AT}^{mnm} W_{mol} / (\rho_M V_{mnm})$, here N_{AT}^{mnm} is the (total) *number of atoms* in the given monomer, and V_{mnm} is the *monomer volume* (tabulated for some well-known polymers elsewhere in the Table 19.2 of the ref. [2].see also beginning of the sub-section 2.2, and Tables 1-4 therein) [2]. This 'alternative' definition of the C_1 coefficient is linked more straightforwardly to the specific polymeric parameters, listed – in particular – in the aforementioned tables, and eventually makes dimension of the 'outcome' of the Eq. (38) to be of [J / (K * mol)], which allows one to compare them directly to the experimental $C_p(T)$ quantities (dependencies), tabulated and plotted for a dominant majority of polymeric materials: see, for instances refs, and also Figure. 3(a) – 6 above. However, in such a case, the C1 meaning could not be identified with the DOS one any more. The latter definition of the C_1 coefficient with the *omitted* W_{mol} term allows one to express the $C_p(T)$ quantities in the [J / (K * g)] units [44-51].

The Emin and Z_{1D}^N quantities incorporated into the Eq. (38) are customarily defined as follows, see also references therein [16]:

$$E_{min} = \frac{2hc_{eff}}{L_z}, \quad (38a) \qquad Z_{1D}^N = \left[L_z\left(\frac{k_B\,\theta_D}{hc_{eff}}\right)\right]^N. \quad (38b)$$

The p_{max} number in Eq. (38) is defined as follows: p_{max} = *floor* ($k_B\,\theta_D$ / E_{min}); where θ_D is the Debye's temperature of the polymeric material [16]. The Eq. (38) allows significant simplification, revealed elsewhere in: {4 * *exp*(x) / [*exp*(x) – 1]^2} → *csch*^{2}(x/2), with the *dimensionless* $x = \hbar\,\omega / k_BT) = (p\,E_{min} / k_BT)$ quantity [29]:

$$C_p^{1DGSM}(T) \cong \frac{k_B\,C_1}{4}\sum_{N=1}^{N_M}\sum_{p=1}^{N\,p_{max}}\frac{csch^2\left(\frac{p\,E_{min}}{2\,k_BT}\right)}{N!\;Z_{1D}^N}\left(\frac{p\,E_{min}}{2\,k_BT}\right)^2\left[floor\left(\frac{L_z}{a_l\,N}\right)\right]^N. \quad (38c)$$

The Eqs. (38 – 38c) depict LA and TA contribution(s) to the lattice thermal capacity of linear polymeric chain(s). Those contributions are formalized within framework of 1D GSM using static plane wave basis– in the apparent similarity with the well-known Debye's formalism of the lattice thermal capacity of bulk solids [16,30].

Another significant contribution to the lattice thermal capacity of low-dimensional polymers is so-called 'conformational contribution $c_{conf}(T)$, which '...is related to large–amplitude *conformational* motion of polymeric segments, e.g., *rotation* of the chemical groups of the polymeric backbone '[29]. Some typical 'conformational' molecular motions are illustrated in the Figure 7 below.

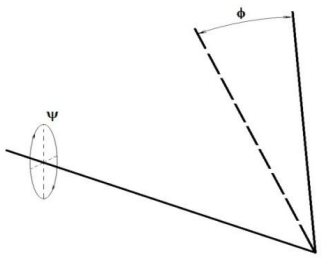

Figure 7: Axial (characterized by the angle ψ) and wagging (specified by the angle ϕ) rotation(s) of a polymeric chain.

In general, there are the 'cooperative' and/or 'non-cooperative' *rotations* of fragments of polymeric chains could be distinguished. In the former case, '…rotation of the one bond or segment does not influence that of its neighbors…' [29]. In such a case, the temperature-dependent 'conformation' contribution to the polymeric thermal capacity reads [29]:

$$c_{conf}(T) = nR_0 \frac{\Gamma\left(\frac{\theta_c}{T}\right)^2 exp\left(\frac{\theta_c}{T}\right)}{\left[exp\left(\frac{\theta_c}{T}\right) + \Gamma\right]^2}, \tag{39}$$

here R_0 is 'universal gas constant', Γ is the 'degeneracy ratio', n is number of *mobile* chain units per repeating unit, while θ_C is the temperature (measured in K) associated with the 'conformation' *non-cooperative* contribution [29]. Typical behavior of the $c_{conf}(T)$ function is illustrated in the Figure 8 below. The nR_o product in the *latter equation* has to be replaced with the Boltzmann's constant, k_B, at its practical implementation.

As it is seen from the Figure 8, the $c_{conf}(T)$ functions evaluated based on the Eq. (39) are apparently *asymmetric*, with their peak temperature(s) being in the range of (0.375 ÷ 0.380) of the θ_C quantity when it varies in the range from 1000 K ≤ θ_C ≤ 2000 K. As for *cooperative* rotation(s), the corresponding $c_{conf}(T)$ function is defined by the Eq. (13) in ref. [29]:

$$c_{conf}(T) = N_A \frac{d}{dT}\left[-k_B T^2 \frac{d\left(F_{conf}(T)/k_B T\right)}{dT}\right], \tag{40}$$

here N_A is the Avogadro's constant, and $F_{conf}(T)$ term represents the temperature-dependent (in general) conformation energy [29]. The latter term reads:

$$F_{conf}(T) = -k_B T\left\{\frac{1}{2}\left[1 + exp\left(-\frac{\theta_A + \theta_B}{T}\right)\Gamma + \sqrt{\left[1 + exp\left(-\frac{\theta_A + \theta_B}{T}\right)\Gamma\right]^2 - 4\Gamma\left[exp\left(-\frac{\theta_A + \theta_B}{T}\right) - exp\left(-\frac{\theta_B}{T}\right)\right]}\right]\right\}, \tag{40a}$$

here temperatures θ_A and θ_B characterize energies (temperatures) of the excited and ground states of the 'non-cooperative' rotational motion(s), while meaning of the Γ parameter is the same as it is in the Eq. (39) [29].

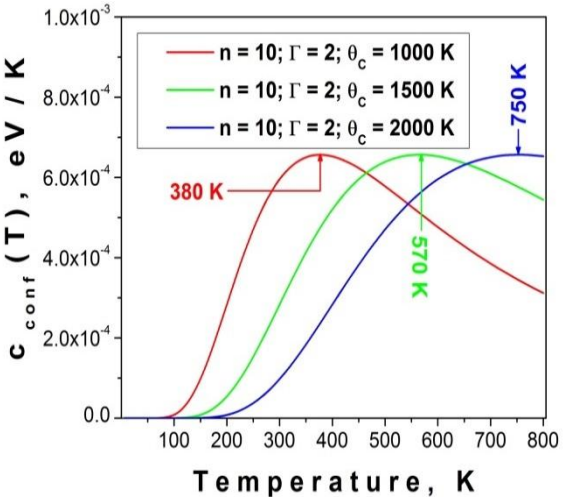

Figure 8: (color online). The temperature-dependent magnitude of the '*non-cooperative*' $c_{conf}(T)$ term, evaluated based on Eq. (39) for three different sets of simulation parameters, shown directly in the figure. Vertical arrows in this figure indicate temperatures, corresponding to the maximums of the $c_{conf}(T)$ dependencies. See main text for details.

It is noteworthy, that all Eqs. (39 – 40a) are obtained using *static rotational* basis. However, the Eqs. (40, 40a) are apparently much *more complicated* than the Eq. (39): the latter equations require consecutive (analytical or numerical) evaluations of two *derivatives* of the temperature-dependent algebraic function(s) with respect to the absolute temperature; therefore, the latter equations will *not* be *used* at $C_p(T)$ simulations herein.

3.2. Simulation Results

The Figures 9(a)-9(h) reveal simulation results (represented with curves) obtained based on the *first term* of the Eq.(38c) for *harmonic* contributions to the experimental $C_p(T)$ dependencies, tabulated for linear polymers elsewhere in refs. [45-48]. Therefore, our simulated $C_v(T)$ curves rather represent temperature-dependent *isochoric* lattice thermal capacities, than the $C_p(T)$ ones, since the *anharmonic* effects (corresponding to higher outer summations terms with N = 2, 3… in the Eqs. (38 – 38c)) are simply omitted at all these simulations. Our simulated $C_v(T)$ curves are also plotted against their appropriate experimental $C_p(T)$ dependencies; see also Figures 3(a), (b) in the *sub-section* 2.3.

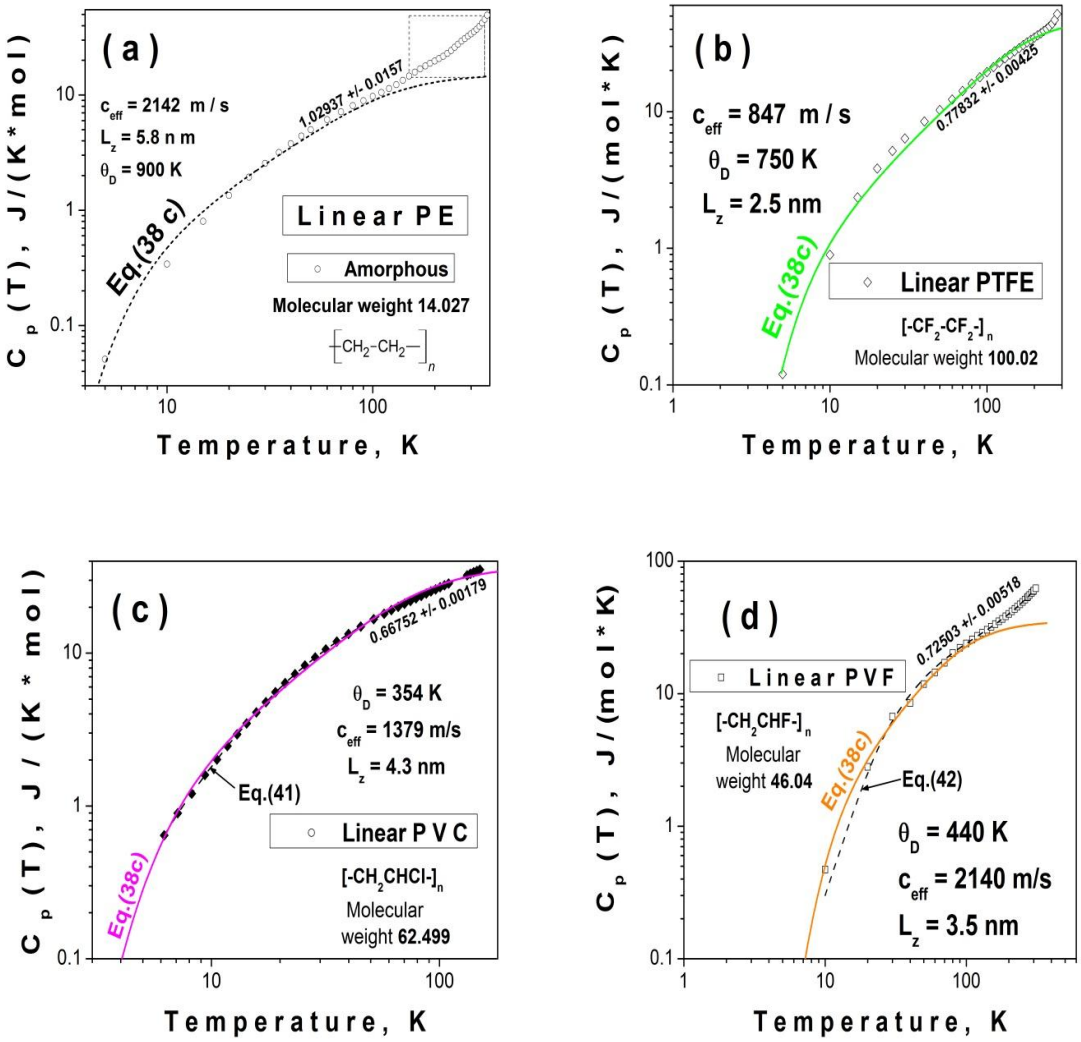

Figures 9(a)–(d): (color online). Symbols: experimental $C_p(T)$ dependencies plotted for linear polymers based on the data tabulated elsewhere in, see also Table 1 and Figures 3(a), 3(b) in the sub-section 2.3. Curves: simulated $C_v(T)$ dependencies, evaluated predominantly based on the very *first term* of Eqs. (38) – (38c). Key simulation parameters are shown directly in the Figures. The dashed rectangular in the panel (a) indicates the 'area ', where the topological amendments in the molecular structure of PE, contribution from its inter-chain interactions, and from anharmonic effects become significant [16,45,46]. See main text for more details.

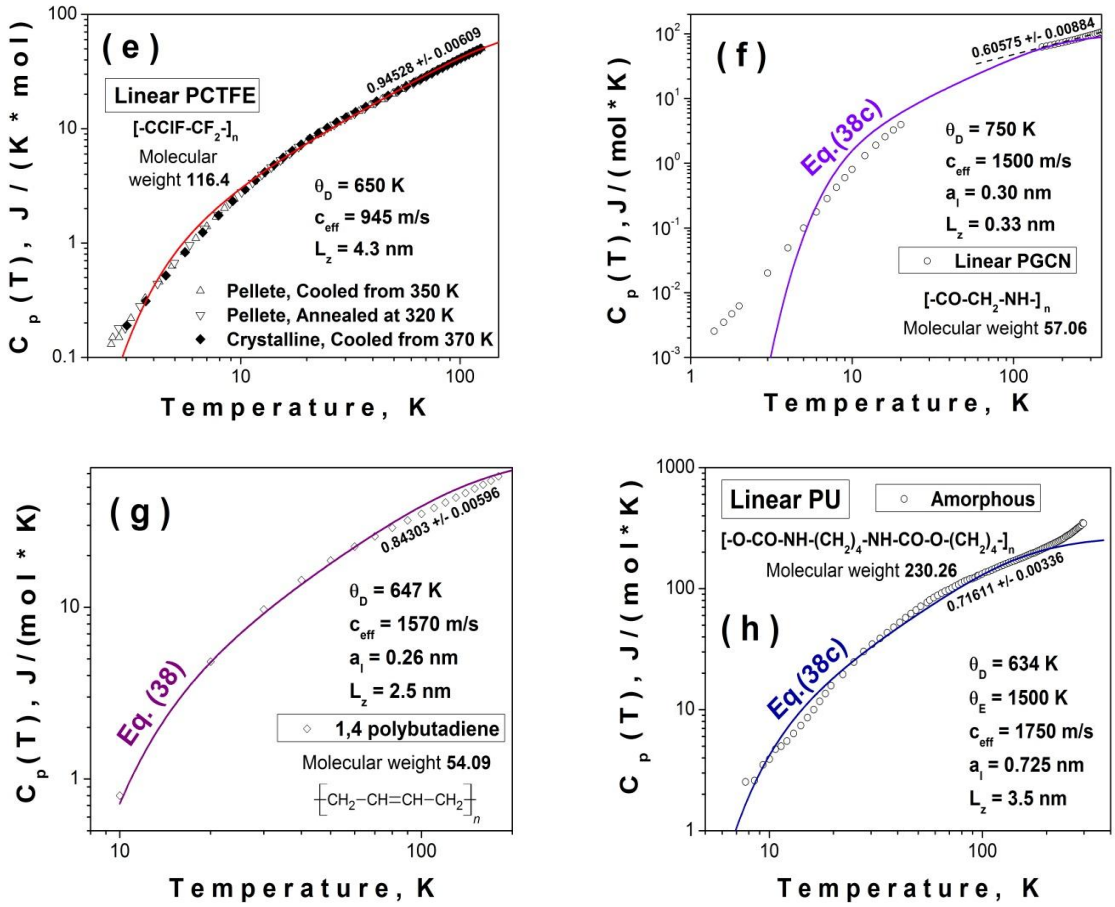

Figures 9(e)–9(h): (color online). Symbols: experimental $C_p(T)$ dependencies plotted for the linear PCTFE, PGCN, PBDN and PU based on the data tabulated elsewhere in, respectively, see also Figure 3(b) in the sub-section 2.3. Curves: simulated $C_v(T)$ dependencies, evaluated predominantly based on the very *first term* of Eqs. (38) – (38c). Key simulation parameters are shown directly in the Figures. See main text for more details [46,48].

As it is seen readily in the Figure 9(a)-9(d), 9(e)-9(h) reasonably well approximation of the *experimental* $C_p(T)$ dependencies obtained for the *linear* polymers with the *simulated* $C_v(T)$ curves (including sub-ranges corresponding to the 'low-temperature anomalies', and those with the (almost) linear $C_p(T)$ and/or $C_v(T)$ enlargement(s)), is achieved (without any further adjustment for the cases with the *dominant contributions* from the *acoustic phonons*!) based on dominant contributions from the 'acoustic' terms, expressed by the Eqs. (38 – 38c).

At the same time, significant contribution(s) the $C_v(T)$ dependencies from so-called 'optical' terms at elevated temperatures (exceeding 250 K) have to be taken account for the data plotted in the Figure 9(h). The latter contribution has been evaluated based on the very first term of the Eq. (38c) at N = 1 and $E_T = \hbar\omega_{opt}$ (here $\hbar\omega_{opt}$ stand for the energies of the optical phonon(s), and – in general – incorporation of the contribution(s) from the optical phonons require some *additional adjustment* for such terms $C_v(T)$ on the vertical scale, in order to match the appropriate experimental $C_p(T)$ dependence [16].

In addition, in the Figures 9(c) and 9(d) both experimental $C_p(T)$ and simulated $C_v(T)$ dependencies are compared as well with their following *polynomial* approximation(s) [46]:

$$C_p(T) = exp[-0.0156374\ (\ln T)^3 - 0.253526\ (\ln T)^2 + 3.38239\ (\ln T) - 5.6602], \quad (41)$$

$$C_p(T) = exp[0.181872\ (\ln T)^3 - \ 2.60825\ (\ln T)^2 + 13.1636\ (\ln T)\ - 19.9019], \quad (42)$$

these equations correspond to the Equations (*b* in the Table 29, and 12) (respectively) in the, and represented with the dashed curve in the Figures 9(c) and 9(d) [46].

Moreover, as it is seen from the Figures 9(a)–9(h), within sub-range(s) corresponding to *elevated* temperatures, significant discrepancies among the experimental $C_p(T)$ curves and simulated $C_v(T)$ ones occurs, and might to be attributed predominantly to significant contributions from the *anharmonic* effects [16,17]. Though those *anharmonic* effects within the *linear* MWs might be – at least in principle – simulated based on the *higher* (the second, third, fourth, etc.) algebraic terms in the Eqs. (38 – 38c) (see also their counterparts in the refs and Figures 9(a) – 10(b) in the illustrations), all those terms are generally expected to yield *linear* in the absolute temperature $C_{ah}(T)$ dependencies for the 1D MWs at their elevated temperatures (see, for instance, Figure(s) 2 in the refs. [19,52-54]).

However, the *experimental* $C_p(T)$ quantities apparently enlarge with this (elevated) temperatures '*superlinearly*': see, in particular, insets to Figures 9(a) and 10(a) as well as the Figures 9(b) and 10(b) in the ref (see also references therein), where the *log-log slop* of the appropriate expe-rimental $C_p(T)$ dependence approaching ~1.44 for the *linear* PE, and ~1.32 for the *branched* PP. In fact, aforementioned discrepancies among predictions of the Eqs. (38 – 38c) and actual behavior of the $C_p(T)$ curves at elevated temperatures could be – in principle – caused by several different reasons [16]. First of all, significant alterations in intensity of interactions among different fragments of the atomic as well as in the molecular structures of PE and PP caused by the temperature enlargement, and even significant amendments in the structural an topological characte-ristics of those macromolecules, especially in vicinity of the temperature(s) of their phase transi-tions (like glass transition temperature, T_g, of PP indicated in the Figures 9(a), (b) of the ref. [16]) could be generally expected at elevated temperatures It is noteworthy, that aforementioned amendments in the topological features of the molecular networks and intensity of inter-action(s) among neighboring fragments of the polymeric chains are expected to affect not only *anharmonic* contributions to the thermal capacity of polymers, but also dominant *harmonic* ones.

In particular, essential features of the $C_p(T)$ and $C_v(T)$ dependencies could be altered due to:
a. Enhanced dynamic *interactions* among *linear* fragments of those macromolecules at elevated temperatures, which were explained and parameterized elsewhere in refs. [8,9]; see also Eqs. (21 – 28) in the sub-section 2.1, and Figures 2(a), (b);
b. Additional structural *entanglement* among neighboring polymeric chains of the linear and branched polymers at their elevated temperatures, with subsequent significant amendments in the *topological* ('*fractal*') characteristic of their molecular network(s);
c. Formation of relatively small fraction(s) of crystalline, amorphous, and even liquid *nano-clusters* (nuclei of the new phases) of essentially different spatial dimensionalities (e.g., 2D, 3D), embedded in the predominantly *linear* topological network(s) of those polymers in vicinity of *temperatures* of their *phase transitions*.

The contribution(s) from the *interaction* term(s) (denoted as the $C_\perp(T)$ one(s) in the Eqs. (22 – 28)) yield either $C_\perp(T) \propto T^{1/2}$ (see Eq. (25) above), or $C_\perp(T) \propto T^{3/2}$ (Eq. (24)), or $C_\perp(T) \propto T^{5/2}$ (Eq. (23). In fact, all those interactions might cause an additional non-linear contribution to the $C_p(T)$ and/or $C_v(T)$ dependencies, which – at least on a qualitative level – explains enlargements in the log-log slop(s)

of the harmonic fraction of the experimental $C_p(T)$ dependencies, obtained for the PE and PP at their elevated temperatures.

Effect of the temperature-induced *entanglement*(s) among the neighboring chain of the fractal and linear polymers, and caused by its amendments in the *fractal dimensionality* of their molecular networks could be depicted quantitatively based on the following equation for the (*harmonic*) $C_v(T)$ dependence is expected for the solid polymer(s) [48]:

$$C_v(T) = 3k_B N_M \mathfrak{D}\,(\mathfrak{D}+1)\,\Gamma(\mathfrak{D}+1)\,\xi(\mathfrak{D}+1)\left(\frac{T}{\theta_{max}}\right)^{\mathfrak{D}}, \quad (43)$$

where $\mathcal{D}$ is the '*fractal* 'dimension of the polymeric structure, N_M is number of the 'particles 'in its 'molecule', $\Gamma(\mathcal{D}+1)$ is the Euler's Gamma-function, and $\xi(\mathcal{D}+1)$ is the Rieman's ξ-function, while θ_{max} stands for a 'characteristic temperature; see also references therein; the $\theta_{max} \cong \theta_D$ equality could be assumed for many practical cases. Based on the latter equation, the log-log *slope* of the *harmonic* fraction, $C_v(T)$ *at elevated temperatures* simply *equals* to the *fractional dimensionality,* $\mathcal{D}$, of the polymeric network: i.e., of $\mathcal{D} \cong 1.44$ for the case of PE, and of $\mathcal{D} \cong 1.32$ for the case of PP. Thus, the temperature-induced additional entanglement among the neighboring linear fragments of polymeric macromolecules is generally expected to increase eventually the log-log slope(s) of both $C_p(T)$ and $C_v(T)$ dependencies, reported for the linear PE and branched PP; see also references therein [16,48].

Appearance of a significant concentrations of the nano-scaled 2D and 3D clusters (nuclei of those new phases) in the temperature ranges close to the temperature of appropriate phase transition within predominantly *linear* structural network(s) of the 1D and branched polymers might also contribute to the amendment in the $C_p(T)$ and $C_v(T)$ dependencies see, for instance, Eqs. (11, 12) elsewhere in the ref, as well as comments to them, and references therein. Moreover – in a substantial distinction from the two aforementioned approximations – in such a case – contributions to both purely harmonic and anharmonic fractions of the lattice thermal capacity of the amended polymeric framework(s) might be evaluated independently [16]. However, quantitative simulation(s) of the log-log slope(s) of those $C_v(T)$ and/or $C_p(T)$ dependencies would require fairly accurate estimation(s) on the actual features of morphology of aforementioned 2D and 3D nano-clusters (nuclei), their temperature-dependent (in general) shapes, concentrations, etc. This information is simply *not available* for the linear and branched polymers, with their experimental $C_p(T)$ and $C_v(T)$ dependencies, reported elsewhere for the in the refs. [45-49]. Therefore, this approach to interpretation on the '*superliner*' behavior of the experimental $C_p(T)$ dependencies will not be discussed any further herein.

Nevertheless, implementation of appropriate combination(s) of the described above simulation approaches, predominantly based on *quantized* and essentially 1D Eqs. (38 – 38c) with explicitly incorporated the dominant *confinement length*, yield fairly good (in general) approximation for the experimental $C_p(T)$ dependencies reported for linear polymers within almost entire temperature range, available for the experimental studies. This indicates overall *correctness* of the implemented simulation approach, as well as importance of the quantum confinement phenomenon for appropriate understanding of the experimental results, reported for many *linear* (chain) polymers.

However, actual situation could be more complicated for *branched* and cyclic polymers, where topology of the molecular structure(s) apparently differs from the linear one(s). The Figures 10(a)-(f) compare experimental $C_p(T)$ dependencies reported for some well-known branched polymers with their simulated counterparts, obtained predominantly based on the Eq. (38c). It is noteworthy, that for the cases of PMA and PMMC, additional 'optical' and 'rotational' terms have to be incorporated as well in order to approximate the experimental $C_p(T)$ curve reasonable well: see Figures 10(d), and 10(f). The latter term is evaluated based on the Eq. (39) with the 'fitted' θ_E and θ_c quantities, indicated directly within the figure. The dashed curve in the Figure 10(c) corresponds to the polynomial approximation, specifies by the Eq. (33): see also comments to the Figure 3(b) above.

As it is seen from the Figures 10(a)-(f), our 1D quantized equation yields, again, fairly *reasonable* overall approximation for the experimental $C_p(T)$ dependencies, reported for *branched* polymers, except the temperature ranges *approaches* phase transition areas, where anharmonic effect(s) [16], as well as – briefly discussed above in this section – topological and structural re-arrangements of molecular network might play significant role(s).

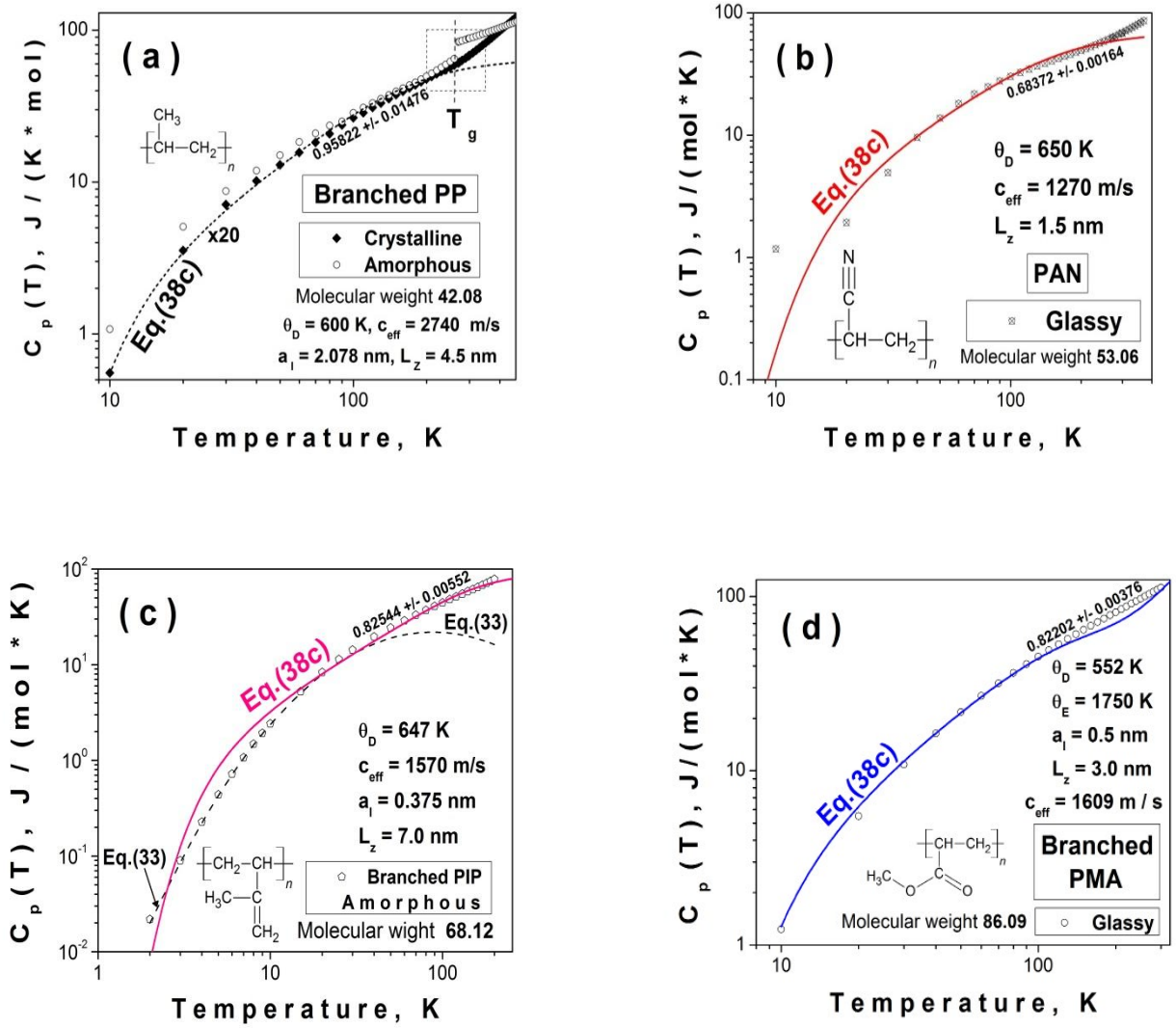

Figures 10(a)–(d): (color online). Symbols: experimental $C_p(T)$ dependencies plotted for *branched* polymers based on the data tabulated elsewhere in refs. [47, 49, 50], see also Table 2 and Figure 4 in the sub-section 2.3. see also refs. [47, 49, 50]. Curves: simulated $C_v(T)$ dependencies, evaluated predominantly based on the very *first term* of Eqs. (38) – (38c). The dashed rectangular in the panel (a) indicates an 'area 'where the topological amendments in the molecular structure of PP, contribution from its inter-chain interactions, and from *anharmonic* effects become significant [16]. Key simulation parameters are shown directly in the Figures. The T_g quantity in the panel (a) corresponds to the 'glass transition 'temperature of 'atactic 'PP; see also references therein. Contribution from the 'rotational 'term is evaluated based on the Eq. (39). Solid figures near the curves indicate log-log slopes of the experimental $C_p(T)$ dependencies at elevated temperatures.

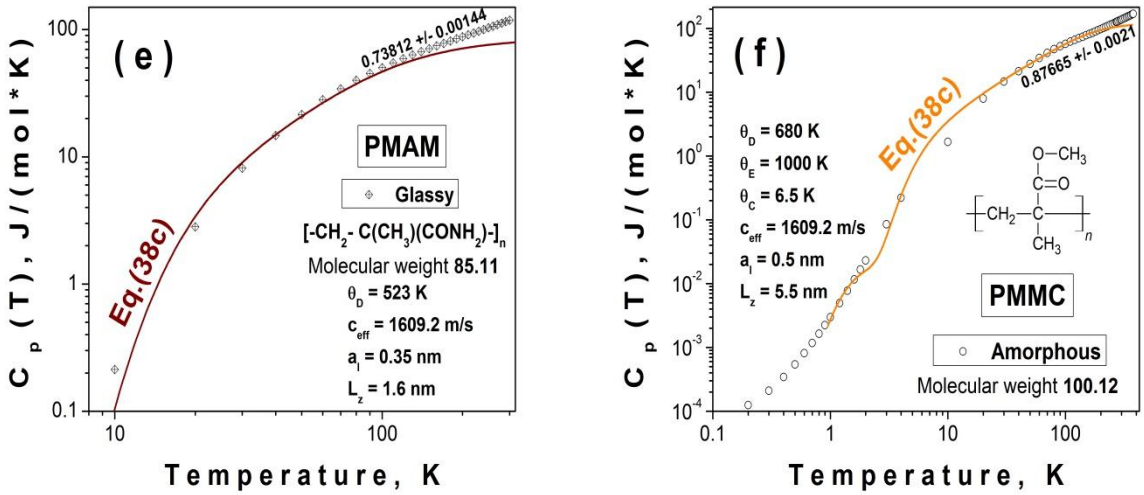

Figures 10(e), (f): (color online). Symbols: experimental $C_p(T)$ dependencies plotted for the PMAM and PMMC based on the data tabulated elsewhere in. refs. [47, 49, 50], see also Table 2 and Figure 4 in the sub-section 2.3 [47,49,50]. Curves: simulated $C_v(T)$ dependencies, evaluated predominantly based on the very *first term* of Eqs. (38) – (38c). Key simulation parameters are shown directly in the Figures. Contribution from the 'rotational 'term is evaluated based on the Eq. (39). Solid figures near the curves indicate log-log slopes of the experimental $C_p(T)$ dependencies at elevated temperatures. See main text for more details.

This indicated that contribution(s) from the 'backbone' acoustic, optical, and even rotational vibrations clearly dominate $C_p(T)$ behavior even for branched polymers, in spite of generally expected significant contribution from the molecular branches of (predominantly) linear 'individual' topology. Such domination could be explained readily, if – assuming relatively short length of (presumably) linear branches and an absence of phonon-phonon interactions (correlations) among the 'backbone' and linear branches (as well as among even neighboring branches themselves) – we compare contribution(s) to the $C_v(T)$ function(s) from the 'backbone' chain(s) and those branches.

Indeed, as it is shown elsewhere in the Figure 7(b) of the ref. [16], contribution from the relatively short linear branches would be significant only at elevated temperatures, where the 'independent' (within a zero-order approximation) $C_v(T)$ curves originated from the individual 'backbone' chains and those originated from these branches would be 'averaged' linearly in accordance to their *relative fractions* (molecular weights) in the total weight of the macromolecule of the given branched polymer (with the anticipated $C_v(T)$ behavior close to the *linear* one at the elevated temperatures) [16]. In such a case, the experimental $C_p(T)$ behavior within the temperature range, corresponding to the 'low-temperature anomalies', would be clearly defined by the longest linear molecular chain, which is apparently expected to be the 'backbone' chain for majority of branched polymers: see, for instance, Figure 7(b) of the ref. [16]. However, for so-called 'hyper-branched' (HB) polymers, the 'aggregate' fraction of all (though relatively short) branches in the molecular weight of their macromolecule(s) might exceed well similar fraction of the 'backbone' chain(s) [37].

In such a case, two (or even more) 'low-temperature anomalies might emerge in the temperature dependencies of the heat capacity of the HB polymers, as it was sketched elsewhere in the Figure 7(b) of the ref. [16]. Only in such a case, particular shape of the $C_p(T)$ might indicate presence of the dominant fraction of the branched polymers in the studied polymeric material. When, however, lengths of the 'backbone chain' and branches of the given polymer are well comparable, we would hardly be able to distinguish contributions to the $C_p(T)$ dependence from the 'backbone' and from chain: see the Figure 7(a) in the ref. [16].

As it will be shown shortly below, similar explanation might be *relevant* even for the case of *cyclic* polymers, where topology of the 'core' ('backbone') and branched molecular structures is generally expected to be essentially different.

Indeed, as it is seen from the very first row of the Table 3, molecular structure of monomer of the polystyrene (PS) comprises of 'linear' CH–CH_2 'backbone' chain (which is quite similar to its counterparts in the polymeric structures of PE and PP, revealed in the Tables 1 and 2), though instead of the 'terminal' *hydrogen* atom in the PE and the 'terminal' *methyl group* of the PP, molecular structure of PS monomer (repeat unit) comprises of terminal '*aromatic*' (benzene) ring. Similar topology of the polymeric chain also emerges for the case of Poly-Alpha-Methyl-Styrene (PαMS), though instead of the benzene ring itself of the PS, molecular structure of the PαMS comprises of such ring with attached 'additional' methyl group: see Table 3 for details and illustration(s). It is noteworthy, that the vibrational wavenumber of the 'terminal' hydrogen atom (or C-H bond) is about of 2850–2960 cm^{-1} (or vibrational energy of 245.59 – 255.07 meV) in alkanes and of 3020–3100 cm^{-1} (260.0 – 267.14 meV) in alkenes, which corresponds to the 'optical' phonon (group) vibration energy range. Consequently, in general, confinement length(s) of the LA and TA phonons might be significantly different for those phonons associated with the thermal

vibrations of aromatic (and/or diester) rings, and for phonons involvement into atomic and molecular vibrations of linear 'backbone' chains of PS and PαMS. Situation could be even more complicated for the case of PETF, where the 'aromatic' rings are incorporated into the 'backbone' chain of the macromolecules [2].

As a result, more than one 'low-temperature' anomalies could be distinguished in the experimental $C_p(T)$ dependencies, reported for the PαMS elsewhere in the ref, and replicated in the Figure 5 herein. The first one emerges when the temperature of those polymers drops below ~60 K. This seemingly corresponds to the relatively *small* phonon confinement *size*, which could be associated readily with the 'diameter' of the 'benzene' ring; it (roughly) equals to double lengths of the C-C bond, i.e., just of ~0.3 nm. However, the second 'anomaly' (with the 'onset' temperature ranging from 2 to 4 K) apparently originates from the larger spatial extent of the 'linear' back bone chain of the PαMS, see Figure 5 above [50]. It is noteworthy as well, that the $C_p(T)$ dependence below the aforementioned 'onset' temperature in this figure reveals the log-log slop approaching 3, which corresponds to the well-known 'Debye's law, with $C_v(T) \propto T^3$ [30]. This also implies indirectly that behaviour of the low-temperature $C_p(T)$ branch originates predominantly from contribution from 3D molecular network(s) of the PαMS and PETF. Though the $C_p(T)$ dependence, plotted in the Figure 5 for the PETF exhibits certain similarity with the behaviour of its counterpart plotted in the same figure for the PαMS (especially at temperatures below 10 K), the 'second anomaly' is not articulated so clearly as it done for the case of the PαMS. The experimental $C_p(T)$ dependencies with two low-temperature 'anomalies', reported for the case(s) of PαMS and PETF, are not fitted herein with the relevant $C_v(T)$ curves because of relative complexity of their macromolecules, and necessity to approximate aptly spatial, vibrational and rotational characteristics of relatively complicated structural units of those macromolecules.

Typical experimental $C_p(T)$ and simulated $C_v(T)$ dependencies, obtained for three other cyclic polymers are compared in the Figures 11(a)-(c). As it is seen from the Figures 11(a)-(c), our simulated $C_v(T)$ curves, obtained based on the Eqs. (38c) replicate reasonably well the experimental $C_p(T)$ dependencies for the poly-glycolide (PGL, see Fig. 11(b)) and poly-c-caprolactone (PCL, see Figure 11(c)).

However, more sophisticated experimental $C_p(T)$ dependencies reported for the polystyrene elsewhere in refs (see also Figure 11(a)) require incorporation of additional 'optical' and 'rotational' terms [50,55].

In general, contribution from the acoustic phonons to the simulated $C_v(T)$ quantity is expected to be defined by the *total number* of vibrating atoms, incorporated into the (linear and/or branched) polymeric chain, or – to be more accurate – by the number of their *degrees of freedom*. The latter number is apparently related to the total number of atoms in the molecule in quite a complicated – in general – way, since existence of interatomic bonds makes atomic quantum movement is far more complicated as compared to similar movement(s) of the same but (nearly) unbounded atoms in a gas. Indeed, in the former case, not only vibrational – but also rotational (cooperative or non-cooperative) contributions are widely expected to the total lattice thermal capacity of polymers. Relatively low characteristic temperature, corresponding to the 'rotation' term, indicates dominance of relatively low frequencies of the rotational movement(s), originated apparently from relatively large weight of the molecular fragments involved into the rotational movement [1,2,29]. As for the molecular structure of the monomer of the polyglicolide (PGL), its 6-member ('cyclic ester' – lactone) ring comprises of two embedded oxygen atoms alongside with the four carbon atoms (see fourth raw in the Table 3), while the 'branched' structure of the PGL macromolecule does not contain any 'rings' et al. Therefore, its effective phonon confinement length, $L_z \cong 5.2$ nm Figure 11(b)), is well comparable with that of PS ($L_z \cong 6.0$ nm, Figure 11(a)), where the phonon confinement length is obviously defined by that of the linear 'backbone' chain, rather than the 'diameter' of the rings. In contrast, relatively short confinement length fitted for PCL (with the $L_z \cong 2.7$ nm, Figure 11(c)), indicates significant contribution from the thermal vibrations, confined within its ring, see the last row in the Table 3.

Usually vibrations of the 'terminal' methyl group might be specified as stretching, bending (with typical wavenumber of 1340 cm-1 – 1485 cm^{-1} or vibrational energy of 166.14 – 184.12 meV), wagging, twisting and rocking ones, with the typical vibrational energies ranging from 146.3 meV to 353.1 meV! In other words, though vibrational spectra of the 'terminal' methyl group is more complicated as compared to that of the vibrational spectrum of the single C-H bond, all its characteristic frequencies still belong to relatively *high-frequency* (energy) region. Therefore, those vibrations would hardly contribute to the low-temperature branches of the $C_p(T)$ dependencies, but rather originate $C_p(T)$ *peaks*, contributing to the measured temperature-dependent heat capacity of polymers at their elevated temperatures (typically exceeding 500 K): see, for instance, Figure 11(a) in the refs. [16,19]. Atomic structure and vibrational spectrum of the aromatic and 'cyclic ester' molecular rings are apparently far more sophisticated than those of the single terminal hydrogen atom and even of the methyl group. Therefore, many types of atomic and molecular vibrations are generally expected to exist (excited) in such rings, and – potentially – all of them might contribute to an 'additional '(as compared to that of PE and PP) temperature-dependent (in general) heat capacity of the PS.

Based on well-known Hückel rule, benzene rings are routinely exhibit 'planar' (flat) molecular structures [2]. Thus, in general, atomic and molecular vibrations of the aromatic rings might be formally separated into two groups: '*in-plane*' and '*out-plane*' ones, with the typical wavenumbers of the 1500 cm^{-1} to 1600 cm^{-1} (or vibrational energies of ~186 meV to 198.37 meV) for the in-plane vibrations, and of 690 cm^{-1} to 900 cm^{-1} (or 85.55 meV to 111.6 meV) for the out-plane ones. Similar separation(s) are well-known for many other planar (2D) semiconducting and insulating (nano) flakes, ribbons, etc.: e.g., graphene, layered hexagonal boron nitride (h-BN) ones, etc., see for instance, ref. [56] and references therein. More importantly, that those 'in-plane' and 'out-plane' atomic vibrations are customarily charecterized by the essentially different spatial dimensionalities: 1D for the 'out-plane' vibrations and 2D for the 'in-plane' ones [2,56]. Consequently, the low-temperature branches of the $C_v(T)$ dependencies for those 2D materials are widely expected to be 'linear' ($C_p(T) \propto T$) when originnated from the 'out-plane' vibrations, and 'quadratic' (i.e., $C_p(T) \propto T^2$) – when originated from the 'in-plane' ones [56]. Similarly, contribution from the 'out-plane' vibrations of the aromatic ring(s) is expected to yield linear (in the absolute temperature) fraction of the total $C_p(T)$ dependence, while contribution from the 'in-plane' ones customarily yields 'quadratic' in the temperature dependence of the lattice thermal capacity of the 'cyclic' polymers at relatively low temperatures. In other words, the 'out-plane' contribution(s) from the aromatic rings routinely yields the linear $C_p(T)$ dependence, which is similar to that customarily expected from the linear polymeric chain(s) (MWs) [16].

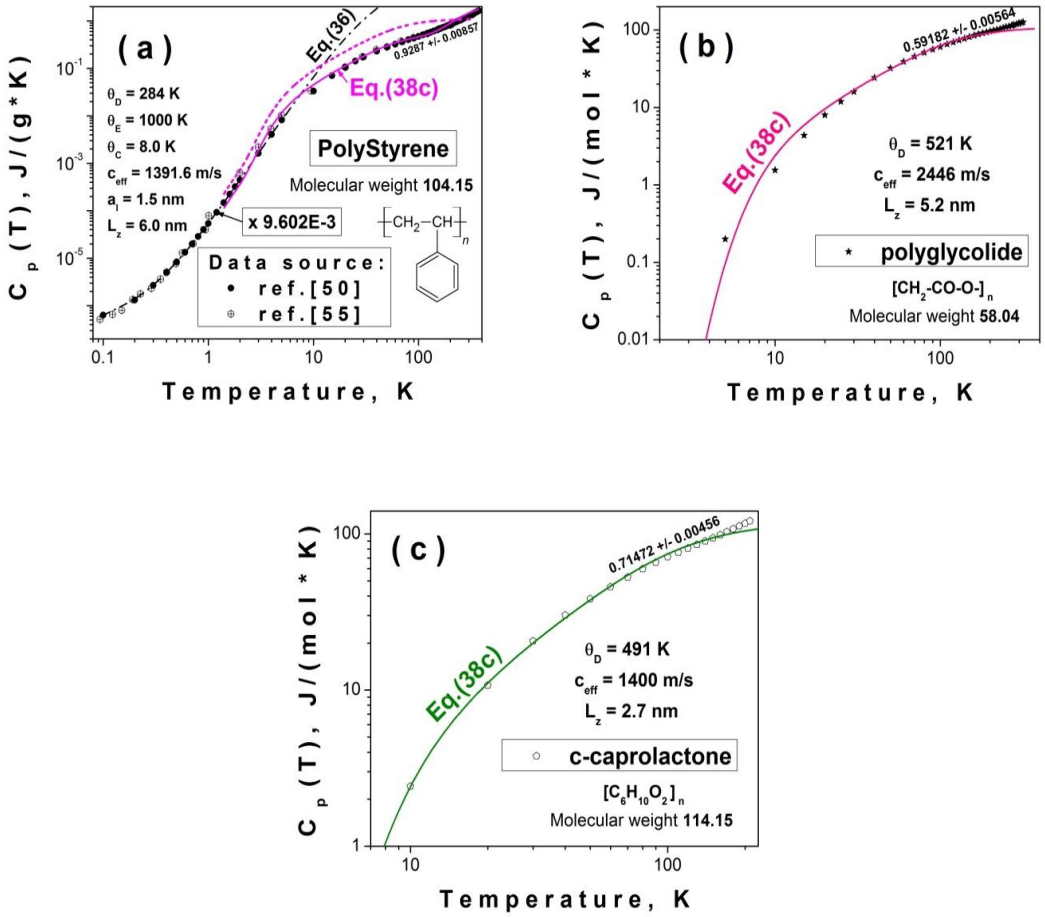

Figures 11(a)–(c): (color online). Symbols: experimental $C_p(T)$ dependencies plotted for *cyclic* polymers based on the data tabulated elsewhere in refs, see also Figure 5 in the sub-section 2.3 [50,51,55]. Original $C_p(T)$ quantities tabulated for PS elsewhere in the ref are normalized by the $9.602*10^{-3}$ constant in order to re-calculate them to the J/ (g * K) scale, adopted for the $C_p(T)$ data in the ref. [50]. Curves: simulated $C_v(T)$ dependencies, evaluated based on the very first term of Eqs. (38, 38c). Key simulation parameters are given directly in the Figures. Contribution from the 'optical 'term in the panel (a) is simulated at the θ_E = 1000 K, while heat capacity of the 'rotational 'term is evaluated based on the Eq. (39) with the characteristic temperature of just θ_c = 8K. Solid figures near the curves indicate log-log slopes of the experimental $C_p(T)$ dependencies at elevated temperatures. Dashed curve in the panel (a) corresponds to the Eq.(38c), re-calculated for the case with the *taken into account contributions* from hydrogen (H) atoms, but at the absence of contributions from the optical phonons, while the solid curve in the same panel corresponds to the case when the contribution from the H atoms are excluded, while the contribution from the optical phonon is taken into account. See main text for more details.

Therefore, the contribution(s) from the linear 'backbone' chain of PS and that from the 'out-plane' vibrations of its 'terminal' benzene ring yields *linear* (in the temperature) terms, which are hardly distinguishable at relatively high temperatures. On the other hand, features of the 'low-temperature anomalies' originated from the linear 'backbone' chain and from the aromatic ring would be apparently defined by the typical spatial extents of aforementioned structural fragments. Such extent of the linear 'backbone' chain is generally expected to be significantly larger (with the typical quantity of ~5–6 nm) than that of the benzene ring (with the 'diameter' of just ~0.3 nm); thus, the length of the 'backbone' chain eventually defines experimentally recorded $C_p(T)$ behavior in this temperature range, see Figure 11(a). As for contribution from the 'in-plane' vibration of benzene ring into low-temperature heat capacity of the PS, it is generally expected to be quite negligible, due to relatively fast decline of the $C_p(T) \propto T^2$ function with the temperature diminishment. In other words, in spite of essential differences in the structural features and vibrational spectra of the linear (e.g., PE) polymeric 'chains' (MWs), and those of the branched (e.g., PP) and even cyclic (e.g., PETF, PαMS, PS) polymers, behavior of their low-temperature $C_p(T)$ and $C_v(T)$ dependencies would be eventually defined by the largest spatial extent of their linear molecular sub-structures, which could be identified often as the length of the linear 'backbone' chain(s). This explains naturally appearance of the common features of the low-temperature parts of the $C_p(T)$ dependencies for all aforementioned polymeric structures: see particularities of the 'low-temperature anomalies' in $C_p(T)$ dependencies in the Figures 9(a)–9(h) for some well-known linear polymers, in the Figures 10(a)-(f) for some branched ones, and Figures 11(a)-(c) for those features of few cyclic polymers. Furthermore, all those common features (including their pronounced 'low-temperature-anomalies') could be replicated reasonably well based on the essentially same simulation approach, which is based on the Eqs. (38 – 38c). These equations are 'designed' for realistic quantitative evaluations on the $C_p(T)$ quantities obtained experimentally for the linear polymeric chains (MWs), and based solely on energetic characteristics of the spatially confined 1D LA and TA phonons, though some corrections with additional 'optical' and 'rotational' terms are apparently required for polymeric structures with the relatively long 'backbone' chins: see, for instance, Figures 9(h), 10(d), 11(a).

It is noteworthy as well, that the *quantum* atomic movement at relatively low temperatures (well below the Debye's temperature of the low-dimensional polymers) within the polymeric macromolecules and monomers is expected to involve predominantly relatively *heavy* carbon (as well as oxygen, nitrogen, chloride, fluorine, etc., atoms) with relatively *low vibrational eigenenergies*, while substantial involvement of quantum motions (modes) related to the comparatively light hydrogen atoms is generally expected mainly at elevated temperatures [40]. This implies, that at our simulations, the N_{AT}^{mnm} quantity, incorporated into the Eqs. (38, 38c) (see also the fifth columns in the Tables 1-4) might be rather associated with the number(s) of relatively heavy *carbon* (as well as of chlorine, nitrogen, oxygen, etc.) atoms embedded into the monomer, than to its total atomic number. As it is revealed in the Figure 11(a) above, this 'alteration' might yield significant *improvement* in the approximation of the experimental $C_p(T)$ data with the simulated $C_v(T)$ dependencies, especially at relatively low temperatures.

The Figures 12(a), (b) show experimental $C_p(T)$ and simulated $C_v(T)$ dependencies, obtained for two simplest *aminoacids*. As it is seen from the Figures 12(a), (b), implementation of appropriate combination(s) of Eqs. (38, 38c, 39) yield reasonably good approximation of the experimental $C_p(T)$ dependencies reported both for the poly-L-alanine-alpha (see Figure 12(a)) and poly-L-valine (Figure12(b)). It is noteworthy to recall, that all three aforementioned equations are obtained merely based on the vibrational and rotational characteristics of individual (and presumably) non-interacting linear macromolecules. However, as it is illustrated in the Table 4 above, monomers of both mentioned above aminoacids contains oxygen and nitrogen atoms as well (alongside with the very common for polymers carbon and hydrogen ones), which eventually originate significantly different local electrical charges of such atoms as compared to those of their neighboring carbon and hydrogen atoms, and their 'electronegativities, as well as – eventually – to the 'ionicity' of the C-O, C-N and C-H bonds, and their significant dipolar (dynamic) electric moments, associated with the presence of such polar covalent chemical bonds [39,57,58]. Indeed, so-called 'Pauling's electronegativity' of the hydrogen, carbon, nitrogen and oxygen atoms are of 2.2, 2.55, 3.04, and 3.44 units, respectively [58]. These differences would originate both (long-range in its nature though 'screened' repulsive and/or attractive) directs Coulomb interactions among all locally charged atoms in the zwitterionic polymeric macromolecules, as well as among significant dipolar moment of the C-O, C-H, and C-N bonds in the polymeric chains of the poly-L-alanine-alpha and poly-L-valine. It is noteworthy, that the non-vanishing though relatively weak dipolar moments of the multiple C-H bonds (due to the electronegativity difference of the carbon and hydrogen atoms of just ~0.35) of any polymeric macromolecule are generally expected for all polymers. Those dipolar momentums might interact (mainly via the Coulomb mechanism) among similar momentums of neighboring C-H bonds, as well as with such momentums of other polar chemical bonds both within individual macromolecules and among neighboring polymeric chains [39,58].

In general, the dipolar moments of chemical bonds are expected to be *dynamic* (time-dependent) due to apparent involvement of all polymeric atoms and chemical bonds among them in the longitudinal and especially 'optical' (group) vibrations at any finite temperature [16].

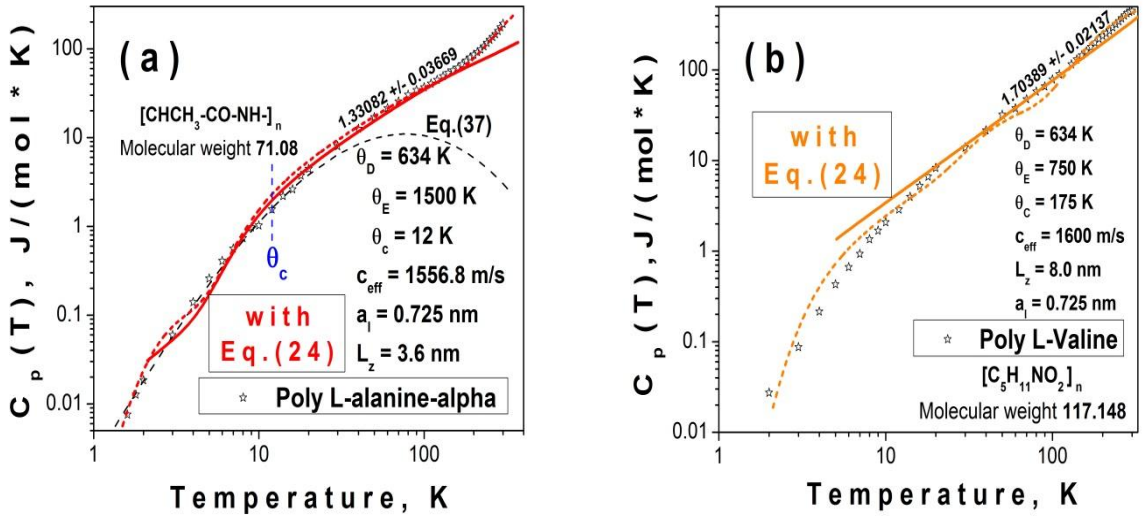

Figures 12(a),(b): (color online). Symbols: experimental $C_p(T)$ dependencies plotted for *two simplest aminoacids* based on the data tabulated elsewhere in refs. [8, 9], see also Figure 6 in the sub-section 2.3. Dashed colored curves: simulated $C_v(T)$ dependencies, evaluated predominantly based on the very *first term* of Eqs. (38, 38c, 39). Key simulation parameters are given directly in the Figures. Contribution from the 'optical 'term reflected in the panel (a) is simulated at the θ_E = 1500 K, while the additional heat capacity of the 'rotational 'term is 'fitted 'with the characteristic temperature of just θ_c = 12 K. For comparison, reasonably accurate 'fit 'to the experimental $C_p(T)$ data plotted in the panel (b) requires the following 'additional 'parameters: θ_E = 750 K and θ_c = 175 K. Solid colored curves in both panels: simulations carried out based on Eq. (38c) with additional 'interaction 'term(s), $C_{\perp}(T)$, evaluated based on the Eq. (24). Solid figures near the curves indicate log-log *slopes* of the *experimental* $C_p(T)$ dependencies at elevated temperatures. See main

Therefore, more appropriate simulation approach might be implemented in these particular cases in order to take into account effect polyof aforementioned (Coulomb) interactions among neighboring MWs. In particular, Eqs. (23 – 25) from the sub-section 2.1 (see also original forms of those equations in the refs. [8, 9]) have to be added to the basic set of equations, required for appropriate simulations on the $C_p(T)$ dependencies poly-L-alanine-alpha and poly-L-valine: the Eq. (24) is used in our particular case: see color solid curves in Figures 12(a), (b); see also caption(s) to them refs. [8,9].

The contribution(s) from the vibrational states confined *within* the molecular wires (MWs), $C_{\parallel}(T)$, combined with those from *interactions* among neighboring MWs, $C_{\perp}(T)$, yield(s) reasonably good approximation(s) of the experimental $C_p(T)$ dependencies at temperatures exceeding ~(5 – 10) K, even though the 'rotational' and 'optical' terms are excluded from the set of simulation equations: see solid colorful curves in the Figures 12(a), (b). These eventually imply, that reasonably good approximations(s) of the experimental $C_p(T)$ dependencies reported for the linear, branched, and cyclic polymers might be achieved predominantly based on the basic equations of 1D GSM model, expressed by the Eqs. (38 – 38c) herein, though – in many cases – additional contributions from the 'intra-chain' 'optical' and rotational terms have to be taken into account rigorously. Moreover, for the case of two simplest amino-acids, convincing approximation(s) for the experimental $C_p(T)$ dependencies might be achieved via implementtation(s) of two *alternative* approximation(s).

The first one is based on assumptions (see result(s) of its implementation plotted with dashed colorful curves in the Figures 12(a), (b)) that all (though different in their physical nature) contribution(s) to the lattice thermal capacity of polymeric MWs essentially originate from the atomic and molecular vibrations *located* (confined) *within* the same *linear* polymeric MW, while the second approximation (which incorporates essentially Eq. (24) into the basic set of simulation equations) presumes substantial (predominantly Colombian in nature) interactions among those vibrations located (confined) within neighboring MWs. Therefore, the 'low-temperature' anomalies are generally expected to be 'retained' even in such a case. When, however, the 'fractal theory' of the lattice heat capacity of polymers becomes valid, the 'low-temperature' $C_v(T)$ dependence, depicted by the Eq. (43) above in this section is expected for the solid polymer(s) [48].

On the other hand, log-log *slop* of the $C_v(T)$ dependence, defined by the 'fractal' Eq. (43) above in this section, becomes *fractional* (i.e., non-integer), and equals to the 'fractal 'dimension of the polymer, *D*. Therefore, this slop is expected to be of $D = 1.64 \pm 0.08$ for the 'bottle-brush' polymeric macromolecules, described, for instance, elsewhere in the ref; see also references therein. This quantity does not deviate drastically from the log-log slope(s) of experimental $C_p(T)$ dependencies reported for the poly-L-alanine-alpha and

elsewhere in the ref. [38], see also Figures 6, 12(a), and 12(b) herein. Indeed, the $D = 1.64 \pm 0.08$ quantity obtained in the ...ref. [38] for the 'bottle-brush' macromolecules lies between the ~1.33 slope evaluated for the $C_p(T)$ dependence reported for the poly-L-alanine-alpha (see Figure 12(a)) and that of ~1.70, defined for the similar dependence reported for the poly-L-valine: see Figure 12(a) [38,47].

It is noteworthy as well, that the *fractional* slope(s) of the $C_v(T)$ dependence, predicted by the Eq. (43) for the polymers with the *fractal* molecular structures, and evaluated *numerically* for the experimental $C_p(T)$ dependencies plotted Figures 12(a), 12(b)) for the two simplest aminoacids, are eventually attributed to inter-molecular interactions within the aforementioned polymers. However, those interactions for the 'bottle-brush' macromolecules originate from '…steric overcrowding of the side chains in the densely packed brush...', causing attractions and/or repulsion among '…side chains…' (brunches) of those macromolecules, spatially arranged based on their (roughly) cylindrical symmetry, while in the case of two simplest aminoacids, illustrated in the Figures 12(a), 12(b)), interactions rather occur among their parallel linear ('backbone') chains (MWs), as it is illustrated in the Figures 2(a), (b), in the sub-section 2.1 herein; see also figures presented elsewhere in refs. [8,9,38]. Consequently, basic equations describing aforementioned interactions (as well as their contributions to the lattice heat capacity of aforementioned polymers) turn out to be essentially different as well: the inter-chain interactions are described by Eqs.(22 – 27) herein (see also their original form(s) elsewhere in refs), while Eq.(43) could be used at approximation on the $C_v(T)$ dependencies, expected for the 'bottle-brush' macromolecules – though for a limited temperature range only – corresponding to their 'super-linear' behavior(s) [8,9].

4. Discussion

In general, the phonon 'confinement length', denoted as L_z in Eqs. (38 – 38c), becomes comparable (at list in its 'geometrical' gist) with the nanometer-scaled 'Kuhn length', L_K, of the one-dimensional polymeric chains. Indeed, traditional interpretation of meaning of the 'Kuhn length' as the spatial extent of the 'rigid' – and, therefore, literally linear (in the Cartesian space) – '…statistical segment…' of a polymeric chain, could be comprehended as well as the Casimir length of the 1D MWs, where the phonon scattering occurs only on their edges (ends) [14]. Very close concept of 'coherence length' of non-disruptive propagation of LA and TA phonons (within the 1D polymeric MWs in this particular case) should be credited to T. Skettrup [13]. However, the L_z quantity in Eqs. (38 – 38c) specifies spatial extent of 1D 'phonon confinement', related intimately to the energetic and statistical characteristics of confined 1D LA and TA phonons, rather than to their propagation length alone. Thus, such interpretation of the meaning of the 'Kuhn length' of the linear polymeric chains (MWs) brings in physically more comprehen-sive characterization of such polymers, which now incorporates not only purely 'mechanical' (like 'rigidity' and length) characteristics of polymeric chains, but also their vibrational (i.e., fre-quencies of confined phonons, those of the atomic and molecular vibrations, etc.) and thermal (Debye temperature) parameters, sound velocity, dispersion relation(s), etc. On the other hand, both formalism of (1D) 'Generalized Skettrup Model (1D GSM), and – in particular – that of the Eqs. (38 – 38c), implemented earlier in ref. [16] (see also references therein) valids for crystalline and amorphous 1D chains, and even for a mixture of those fraction.

Strictly speaking, identification of the L_z parameter of 1D GSM as the 'Kuhn length' of poly-meric MWs might not be really meaningful even for many real polymers with the linear molecular structures. First of all – since the 'Kuhn length(s)' for majority of well-known linear polymers (except those of DNA molecules) are typically varying in the range from ~0.8 nm to just below 4 nm (see, for instance, Table 2.1 in the second chapter of the ref. [1], and the Tables 25.1, 25,2, and 25.3, presented in the 25_{th} chapter of the ref. [2]. – significant quantum effects (e.g., penetration of the confined vibrational wavefunction(s) in the 'longitudinal' direction of the MWs beyond the purely 'geometrical' Λ_{Cs} extent) are generally expected [1,2]. Secondly, as it is illustrated in the Figure 13 below, vibrational wavefunctions of the 'freely joined' fragments of the polymeric chains (MWs) might interact with neighboring ones at the ends (joinings) of these neighboring fragments of the MW. Eventually, aforementioned interactions, might affect the 'resonance' characteristics of the confined – within every individual fragment – thermal vibration(s) phonons.

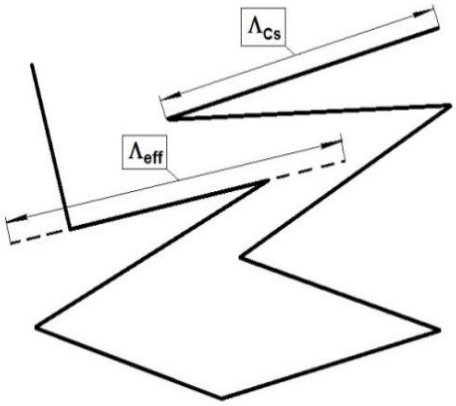

Figure 13: Schematic illustration of key spatial extents in the MWs, composed of linear 'freely joined' fragments. The 'geometrical' – Casimir (Λ_{Cs}) – and 'effective' (Λ_{eff}) lengths of those fragments are also shown for comparison. See main text for more details.

In such situation, the physically meaningful *confinement length*, customarily evaluated for the individual linear fragments (MWs) based on their 'geometrical' spatial extent(s), Λ_{Cs}, has to be replaced with its 'effective' counterpart (Mean-Free-Path, MFP), Λ_{eff}, which could be, for instance, specified as [57]:

$$\Lambda_{eff} = \frac{1+p_r}{1-p_r}\Lambda_{Cs}, \quad (44)$$

here, p_r is the probability of a (LA and/or TA) phonon to be *specularly* reflected on the end(s) of the linear fragment of the MW, Λ_{Cs}, is the so-called 'Casimir' (geometrical) MFP, evaluated based on the assumption of *dominance* of phonon *scattering* on the *borders* (ends) of the linear polymeric fragments, as well as on the *absence* of significant phonon-phonon inter-actions within each *linear* fragment of the MW [57]. In our notations, the *effective* Casimir MFP, Λ_{eff}, simply equals to L_z length, see Eqs. (38 – 38c) and comments to Figure 13.

The $p_r = 0$ in Eq. (44) corresponds to the 'purely *diffusive*' case, while the $p_r = 1$ corresponds to the 'purely *specular* 'one; see also comment to Eq.(2) in ref. [57]. Based on Eq. (44), at $p_r = 0.25$, the Λ_{eff} (or L_z) length becomes by ~1.66 times *longer* than the Λ_{Cs} one. Thus, the physically meaningful spatial extent (length) of the 1D *phonon confinement* within a polymeric MWs is actually defined not only by the geometrical (Casimir) length(s) of its linear fragment(s), but also by inevitable manifestation of the quantum effects in nano-scaled MWs, and by particularities of 'conjugation 'among those neighboring fragments: see Figure 13. The Eq. (44) had been originally intended for evaluation on parameters of thermal transport in 'corrugated' silicon nano-wires (SiNWs) [57]. Though features of phonon confinement within SiNWs of 'corrugated' cylindrical morphology are expected to be defined by its 3D geometry (morphology), the same Equation could be apparently implemented for the1D case(s) of polymeric MWs. Thus, the essentially quantum nature of the confined atomic and molecular vibrations (phonons) and (potential) interference among the vibrational wavefunctions from the neighboring joined linear fragment(s) of linear polymeric chains might amend significantly the actual confinement length of the quantized vibrations as compared to the purely 'geometrical' length(s) of those linear fragments [57].

In other words, their actual length(s) of spatial confinement might (and actually should) *differ* considerably from their (defined predominantly in an essentially 'statistical' manner) 'Kuhn length(s)', though – in general – both lengths are obviously expected to be fairly close to each other. It is noteworthy as well, that in the polymeric chains composed of linear fragments of not-exactly-*equal* lengths, the 'effective' L_z (or Λ_{eff}) quantity could be obtained via appropriate 'averaging' procedure; see brief discussion on this issue in comments to Figures 10(a), (b) in the **previous** section, and more detailed one in elsewhere in the ref. [16]. More complicated topology of polymeric macromolecules of polyethylene terephthalate (PETF) comprises of benzene *ring*(s) embedded directly into the 'backbone' chain: see Table 3 for illustration.

Incorporation of the temperature-dependent '*free energy* of *confinement*', $F_{cnf}(T)$, of the polymeric chain within a *cylindrical* or *rectangular* 'tubes' (see, for instance Eq. (17) in the sub-section 2.1 herein and ..ref. [26] for further details) in the basic set of equations, used at simulations on the $C_v(T)$ and/or $C_p(T)$ dependencies of the low-dimensional polymers, would apparently bring-in the linear (in

the temperature) additional contributions to those $C_v(T)$ and/or $C_p(T)$ dependencies. Thus, appearance of those additional contributions (terms) are not expected to amend the generic linear character of the low-temperature branches of the $C_v(T)$ and/or $C_p(T)$ dependencies, predicted – based, for instance, on 1D version of the well-known Tarasov's equations, and even from Eqs. (38 – 38c) – for the linear polymers [26]. On the other hand, aforementioned Eq. (17) does not predicted any $F_{cnf}(T)$ contributions to the non-linear $C_v(T)$ and/or $C_p(T)$ declines with the diminishment in the absolute temperature(s) of the polymers. In other words, this temperature-dependent 'free energy of confinement' term(s) will not replicated the 'low-temperature anomalies', well documented for all LP studied herein: see Figures 3(a), (b) in the sub-section 2.3, as well as original references with the tabulated 'recommended' $C_p(T)$ data for the LP. Thus, the $F_{cnf}(T)$ term, defined by the Eq. (17) is not linked et all to the well-known confinement phenomenon of the LA and TA phonons, located within linear fragment(s) of MWs, and closely related to them 'low-temperature anomalies' of the $C_v(T)$ and/or $C_p(T)$ curves. In contrast, the implementation of the combination of the Eqs.(38 – 38c) replicates readily those 'low-temperature anomalies' based on the presumption of existence on the energy 'gap' in the vibrational spectra of low-dimensional polymers, incorporated naturally into those equations: see Figures 9(a)-12(b) above. Width of this 'gap' is inversely proportional to the confinement length, L_z, embedded routinely in all those equations (see, in particular, Eq. 38(a) and comments to it at the beginning of the sub-section 3.2), and this gap *vanishes* for an *infinitely long* linear MWs.

The Figure 14 reveals $L_K(L_z)$ dependence of the Kuhn length, L_K, reported (predominantly) elsewhere in the Chapter 2 of the ref. [1], of the ref. [2], versus the L_z quantities, obtained via fitting of the simulated $C_v(T)$ curves obtained based on the Eqs. (38 – 38c) to their experimental $C_p(T)$ counterparts, see Figures 9(a)-12(b). As it is seen from the Figure 14, the L_K and L_z quantities obtained (via the GSM simulations) for the Linear Polymers (LPs), Branched Polymers (BPs), Cyclic Polymers (CPs), as well as for the simplest amino-acids (AA) could certainly be characterized as 'correlated' ones, though this correlation is apparently not of the 'global' type: i.e., it could not be established in a 'universal' way, pertinent for all points revealed in the latter Figure. However, for two 'sub-groups' (marked out as the I – first, and II – second) of the LPs, BPs, and CPs, the $L_K(L_z)$ dependences could be approximated with the linear inclines, but of two essentially different slopes. The higher slope evaluated for the first (I) group indicates fairly straightforward relation among the L_K and L_z quantities, while the lower (second, II) slope indicate significant differences among purely (classical) mechanical L_K quantities and quantum-mechanical L_z ones. It is noteworthy, that the separation of the $L_K(L_z)$ dependences in Figure 14 into two distinctive sub-groups obviously is not originated by the particularities of molecular topology of the studied polymers: the LP, BP and CP 'representatives' appear both in the *first* (I) and the *second* (II) sub-groups.

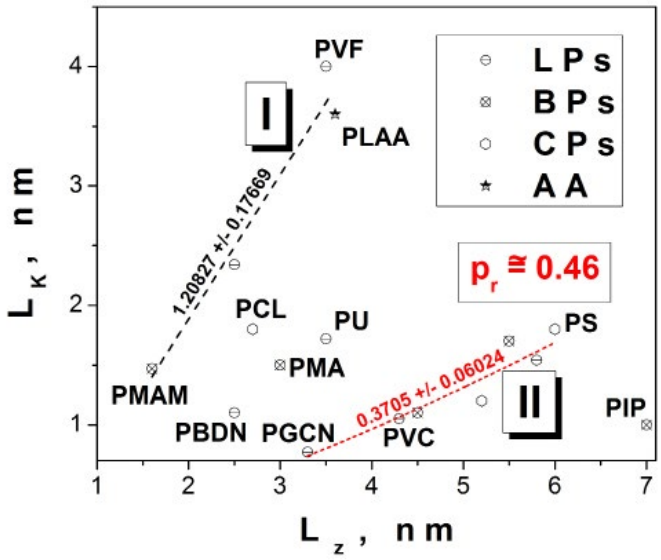

Figure 14: (color online). The Kuhn lengths, L_K, of different polymers, plotted against the L_z ones, used at simulations of the $C_v(T)$ dependencies revealed above in the sub-section 3.2 in the Figures 9(a) - 12(b). The L_K quantities implemented in this particular figure are (mainly) reported for the Linear Polymers (LPs), Branched Polymers (BPs), and Cyclic Polymers (CPs), elsewhere in the Tables 25.1, 25.2, and 25.3 presented in the 25th Chapter (by L. J. Fetters, D. J. Lohse, and R. H. Colby) of the ref. [2]. Polymer abbreviations are explained in the Tables 1-4 herein; see the sub-section 2.2. Majority of open symbols revealed in this figure are 'clustered' in two sub-groups, indicated as I and II in the figure, with (approximately) *linear* inclines of the $L_K(L_z)$ dependencies. Their averaged slopes are evaluated using standard least-square-fit procedure(s), and indicated directly in the figure. The p_r quantity for the second (II) group is estimated based on the Eq. (45). See main text for more details.

Instead, the differences in the $L_K(L_z)$ slopes within these two sub-groups could be rather related to particularities of vibrational wavefunctions, confined within MWs of different topology, and interpreted readily based on the Eq. (44) above. Indeed, if the contribution from the *quantum interferences* among confined vibrational wave-functions on the edges of freely joined segments of the polymeric chains (MWs) are expected to be relatively weak, then the (approximate) $L_K \cong L_z$ equality is generally expected based on the Eq. (44). This is the case, 'represented' by the (first, I) sub-group of $L_K(L_z)$ points with the linear incline, revealed in the Figure 14. When, however, quantum interferences become significant, the 'effective' MFP, Λ_{eff}, (and the effective phonon confinement length, L_z) could *differ significantly* from the 'geometrical' (Casimir) Λ_{Cs} length, as it is revealed in Figure 13.

In the latter cases, actual *spatial extent* of the *one-dimensional* (linear) confinement of the LA and TA vibrations, L_z (or Λ_{eff}) embedded into the basic equation(s) of the 1D GSM, it is generally expected to correlate (though not really coincide) with the Kuhn length, L_K, of the linear polymeric chain(s). In such a case, Eq. (44) above could be 'inverted' readily in order to estimate the *effective* p_r quantity based on the (presumably) known L_z and L_K values:

$$p_r = \frac{|r_L - 1|}{r_L + 1}, \quad (45)$$

with the (averaged) r_L ratio defined as follows: $r_L = \langle L_z \rangle / \langle L_K \rangle$, i.e., based on appropriately 'averaged' L_z and L_K quantities, see also explanations of the of the L_z (Λ_{eff}), and L_K (Λ_{Cs}) parameters in the comments to the Eq. (44) above, and the Figure 13 for illustration. Vertical brackets in the re-numerator symbolizes its absolute value. Implementation of Eq. (45) yields: $p_r \cong 0.459$ for the second sub-group of the points in the Figure 14, at the $r_L \cong 2.70$, defined by the '*inverse*' average slop of the $L_K(L_z)$ dependence, evaluated for the points for the second (II) sub-group of the plot. This indicates relatively high 'transparency 'of the 'borders '(ends) of the linear fragments of jointed MWs for the (still confined – though with much longer – by ~2.70 times in this particular case – 'effective 'confinement lengths) LA and TA phonons.

At the same time, the $L_K(L_z)$ points, plotted based on the data evaluated for the linear PBDN, PGCN and PU, as well as for the 'cyclic' PCL do not really belong either of the aforementioned groups of points in the Figure 14. This could indicate presence of significant fractions of MWs composed both of freely joined linear sections (fragments), as well as of spatially 'isolated' (dangling) such section(s), with no attachment(s) to the neighboring sections (fragments) at least at one of their ends. Thus, in the latter case the effect(s) of quantum interference among vibrational wavefunctions on the end(s) of the joined fragments are apparently weakened – or even completely absent, which makes the actual confinement length, L_z, for the wave functions of the LA and TA phonons to be approximately equals to the 'geometrical' (Casimir) length, Λ_{Cs} (or L_K one), of the linear molecular fragments, see group (I) in the Figure14. Thus, the latter Figure illustrates close relationship established convincingly among the L_z length – (which is defined essentially based on a quantum mechanical concept of phonon confinement and closely related to them essentially 'non-classical' phenomena: the 'low-temperature anomalies', contributions (evaluated via calculations on the probability of quantum-mechanical fluctuations) to the lattice thermal capacity of low-dimensional polymer(s), etc.), – with the Kuhn length, introduced many decades ago entirely based on purely classical-mechanical (though very intuitive!) concept(s) of rigidity of one-dimensional polymeric chain(s), length of its 'statistical segment', which manifests '…crossover to the large-scale random-walk behavior…', etc. [1-3,7,15]. Since the persistence length of the polymeric chain(s) – which is well defined within framework of the KP model – is closely related to the Kuhn length of those chain(s) (see, for instance, Eq. (16) in the sub-section 2.1, comments to it, and references therein), some quantum mechanical aspects of the persistence length could be established and discussed as well within framework of the 1D GSM approximation.

In fact, essentially *quantum-mechanical* (e.g., path-integral) approximation(s) were implemented quite long time ago at modelling on different aspects of polymeric structure, topology, dynamic and statistics (see also references therein), though, at Monte-Carlo simulations on the structural and thermal characteristics of polymers, they usually *combined* with their *classical-mechanical* counterparts: 'mass-weighted velocity' autocorrelation function, so-called ''Wigner-Kirkwood expansion' [60, 61], Gaussian fluctuation theory, Neural Network Model [62,63], while in our case the essentially quantum-mechanical approximation could be used as a 'stand-alone' one, though its key parameters (i.e., the spatial extent of one-dimensional phonon confinement, Debye temperature of the polymer, its sound velocity and lattice constant) have to be taken as the 'known' – from other independent sources – estimates. Furthermore, in contrast, to main conclusions resulting from our simulations, with the one-dimensional phonon confinement length, L_z, playing the crucial role, authors of the ref. [62] suggested that '…size of confining surface…' alongside with its morphological characteristics (i.e., '…curvature and shape…') would be more appropriate parameters at quantitative simulations on the statistical characteristics of polymeric chains [59-63].

5. Conclusion

Results of *semi-empirical* simulation on features of *isochoric* temperature-dependent lattice thermal capacity, $C_v(T)$, of low-dimensional polymeric solids of essentially different molecular structures, spatial extents and dimensionalities are presented in this article, and discussed in details in comparison with their experimental isobaric counterparts, $C_p(T)$, reported for several linear, branched, and cyclic polymers, as well as for two simplest amino-acids. Both the experimental, $C_p(T)$ dependences, and simulated $C_v(T)$ ones, reveal sub-linear, nearly-linear, and super-linear enlargements with the temperature at relatively high temperatures (typically exceeding ~50 K), alongside with the pronounced 'low-temperature anomalies': relatively sharp (and essentially non-linear) decline(s) in the isobaric heat capacity of those polymers with the temperature diminishment: see details in the sub-section 2.3. Furthermore, in general, fairly reasonable quantitative agreements have been achieved among the simulated $C_v(T)$ dependencies based on the provided and verified 1D version(s) of the GSM equation(s) without adjustment – at least for the case of the studied above linear polymeric chains with dominant contribution from the quantized acoustic vibrations, and their experimental counterparts, $C_p(T)$, for all aforementioned groups of low-dimensional solid polymers, both at the 'elevated temperatures', as well as within the temperature sub-ranges, corresponding to the 'low-temperature anomalies', see the simulation results in the sub-section 3.2 and detailed discussion in the previous section.

The basic set of implemented simulation equations incorporate as a key parameter the one-dimensional (1D) spatial extent (length) of confinement of LA and TA phonons, located within the linear (straight) fragments of molecular wires (MWs). Moreover, contribution(s) from their 'optical' (with Einsteinian spectrum) and rotational terms (wherever they are necessary), as well as those from interactions among neighboring linear MWs are also incorporated into the basic set of equations implemented at these simulations. Features of revealed herein experimental $C_p(T)$ and simulated $C_v(T)$ dependencies are also discussed in comparison with predictions of some others well-known approximations: 'fractal theory' of heat capacity of polymers, Tarasov's and Stockmayer-Hecht (with Genensky-Newel amendments) equations, as well as contribution(s) from the temperature-dependent 'free energy of confinement'. Notably, that all these well-known theoretical approximations do not incorporate implicitly lengths (spatial extents) of the phonon confinement within the low-dimensional polymeric solids, and – therefore – do not allow one to replicate unambiguously behavior of the $C_v(T)$ and $C_p(T)$ dependencies within temperature sub-ranges, corresponding to the 'low-temperature anomalies.

On the other hand, the persistence, Kuhn, entanglement length(s) (etc.) of the low-dimensional polymeric macromolecules are known as universal characteristics of their structural, topological and classical-mechanical behavior(s) for more than seven decades: see the sub-section 2.1 and references therein for brief review on the history and physical meanings of aforementioned length(s). Institution of those lengths (sizes of the spatial extent) as key structural and topological characteristics of the real low-dimensional polymers manifested important achievements in interpretation of their key structural, mechanical, and other macroscopic properties, and allowed one to establish generic understanding and explanation(s) of quite complicated – in general – features of the linear, branched and cyclic macromolecular solids. Therefore, incorporation of the nano-scaled confinement length(s) of acoustic phonons in a key set of structural, topological mor-phological parameters of those polymers just follows the aforementioned 'tend', and – in a certain sense – develops it even further: brings-in essentially quantum-mechanical description of statistical characteristics of their spatially confined acoustic and optical atomic vibrations. Furthermore, discussed in the previous section inter-relation(s) among the aforementioned well-established structural and topological characteristics (lengths) of different types of polymeric solids and their length(s) of phonon confinement, which also affect(s) straightforwardly other key vibrational characteristics of those polymers, allows one to clarify several important issues regarding intimate relationship(s) among the microscopic (atomistic), and mesoscopic (mono-meric) structural and even macroscopic thermal characteristics of different types of those solids.

In particular, linear correlation(s) among the nano-scaled lengths of 1D spatial confinement(s) of the LA and TA phonons (used at our simulation(s) on the $C_v(T)$ behavior) and the Kuhn (as well as the persistence) lengths of low-dimensional polymers (collected for those polymers from several well-reputable monographs and textbooks) is established convincingly for majority of studied herein solid low-dimensional polymers: please see details in the end of the previous section. This inspire us to discuss traditional meaning of the Kuhn length in a wider context: it could be treated not only as a classical-mechanical (though nano-scaled) length of rigid 'statistical' segment of a polymeric chain, but also as a length defining the actual size of essentially quantum spatial confinement of one-dimensional LA and TA phonons, which eventually delineates behavior(s) of the $C_v(T)$ and $C_p(T)$ dependencies, evaluated for those polymeric chains – especially within the temperature sub-ranges corresponding to their 'low-temperature anomalies' – and, potentially, becomes of significant importance even for characterization of the length(s) and lifetime(s) of phonon-based thermal transport in all those low-dimensional nano-scaled polymeric solids. Thus, presented, analyzed, and interpreted herein simulation results allows one to extend significantly scope of traditional understanding of several key concept(s) of the thermal physic and features of well-known structural models of the low-dimensional and nano-scaled polymers, as well as provide a profound inside into actual roles of their structural, topological and morphological characteristics in 'shaping' of the vibrational and thermal properties of various low-dimensional polymeric solids.

References

1. Rubinstein, M., Colby, R. H., (2003). Polymer Physics, (Oxford University Press), ISBN: 019852059X.
2. Mark, J. E. (2007). *Physical properties of polymers handbook* (Vol. 1076, p. 825). J. E. Mark (Ed.). New York: springer.
3. Van Krevelen, D. W. (2009). (Revised by Nijenhuis, K. Te.). Properties of Polymers—Their Correlation with Chemical Structure; Their Numerical Estimation and Prediction from Additive Group Contributions.
4. Kuhn, W. (1934). Über die gestalt fadenförmiger moleküle in lösungen. *Kolloid-Zeitschrift, 68*(1), 2-15.
5. Flory, P. J. (1975). Spatial configuration of macromolecular chains. *Science, 188*(4195), 1268-1276.
6. Kratky, O., & Porod, G. (1949). Röntgenuntersuchung gelöster fadenmoleküle. *Recueil des Travaux Chimiques des Pays-Bas, 68*(12), 1106-1122.
7. Svaneborg, C., Karimi-Varzaneh, H. A., Hojdis, N., Fleck, F., & Everaers, R. (2016). Multiscale approach to equilibrating model polymer melts. *Physical Review E, 94*(3), 032502.
8. Stockmayer, W. H., & Hecht, C. E. (1953). Heat capacity of chain polymeric crystals. *The Journal of chemical physics, 21*(11), 1954-1958.
9. Genensky, S. M., & Newell, G. F. (1957). Vibration spectrum and heat capacity of a chain polymer crystal. *The Journal of Chemical Physics, 26*(3), 486-497.
10. Tarasov, V. V., & Yunitskii, G. A. (1950). Theory of heat capacity of chain and layer structures. *Zh. fiz. khim, 24*(1), 111-128.
11. Berman, R., & Berman, R., Thermal Conduction in Solids (Clarendon Press, Oxford, 1976) 208 pages, ISBN: 0198514298.
12. Kittel, C. (2005). Introduction to Solid State Physics; Wiley, Hoboken.
13. Skettrup, T. (1978). Urbach's rule derived from thermal fluctuations in the band-gap energy. *Physical review B, 18*(6), 2622.
14. Casimir, H. B. G. (1938). Note on the conduction of heat in crystals. *Physica, 5*(6), 495-500.
15. Ligatchev, V. (2022). Size-dependent thermal capacity of graphene nano-ribbons. AIP Advances, 12(12), 125010 (2022), 7 pages, doi: 10.1063/5.0123567.
16. Ligatchev, V. (2025). Quantitative Evaluations on Harmonic and Anharmonic Lattice Thermal Capacity of Polymers. *Recent Progress in Materials, 7*(2), 1-37.
17. Ligatchev, V (2025), On Experimental Evidences on Existence of Spatial Confinement in Industrial Polymers, accepted keynote talk on International Conference on Materials, Science, Engineering and Technology, Paris, France, 28–30 May; see also pp. 125–126 in the Book of Abstract of the Conference.
18. Demydiuk, F., Solar, M., Meyer, H., Benzerara, O., Paul, W., & Baschnagel, J. (2022). Role of torsional potential in chain conformation, thermodynamics, and glass formation of simulated polybutadiene melts. *The Journal of Chemical Physics, 156*(23).
19. Wunderlich, B., (2005), Thermal Analysis of Polymeric Materials, Springer-Verlag, Berlin-Heidelberg (2005), ISBN 3-540-23629-5.
20. Rosenbaum, J.F., *Bulk Acoustic Wave Theory and Devices, Artech House, Boston,* 1998, 480 pages, ISBN: 978-0890062654 (089006265X)
21. Cheng, C. F., McCraw, T. J., Solomon, T. H., Yan, M. R., Wnek, G. E., Olah, A., & Baer, E. (2024). High elastic modulus polyethylene: Process-structure-property relationships. *SPE Polymers, 5*(3), 366-381.
22. Hsu, H. P., Paul, W., & Binder, K. (2011). Breakdown of the Kratky-Porod wormlike chain model for semiflexible polymers in two dimensions. *EPL (Europhysics Letters), 95*(6), 68004.
23. Kilanowski, H. P., March, P., & Šamara, M. (2019). Convergence of the Freely Rotating Chain to the Kratky-Porod Model of Semi-flexible Polymers: HP Kilanowski et al. *Journal of Statistical Physics, 174*(6), 1222-1238.
24. Kratky, O., & Porod, G. (1949). Diffuse small-angle scattering of X-rays in colloid systems. *Journal of colloid science, 4*(1), 35-70.
25. Everaers, R., Karimi-Varzaneh, H. A., Fleck, F., Hojdis, N., & Svaneborg, C. (2020). Kremer–Grest models for commodity polymer melts: Linking theory, experiment, and simulation at the Kuhn scale. *Macromolecules, 53*(6), 1901-1916.
26. Wang, J., & Li, K. (2019). Statistical behaviors of semiflexible polymer chains stretched in rectangular tubes. *Polymers, 11*(2), 260.
27. Tarasov, V. V. (1953). Heat capacity of chain and layer structures. *Zh Fiz Khim, 27*, 1430-1435.
28. Tarasov, V. V. (1955). Anisotropic atomic vibrations and the heat capacity of layer and chain structures. In *Dokl. Akad. Nauk*. SSSR (Vol. 100, p. 307).
29. Thybring, E. E. (2014). Explaining the heat capacity of wood constituents by molecular vibrations. *Journal of materials science, 49*(3), 1317-1327.
30. Debye, Peter. "Zur theorie der spezifischen wärmen." Annalen der Physik 344.14 (1912): 789-839.
31. Born, M., & Von Kármán, T. (1967). *Über schwingungen in raumgittern.*
32. Born, M., Von K, T., (1913). Zur Theorie der Spezifis chen Waermen, *Physik. Zeits*., 14, 15 – 19.
33. Novikov, V. U., & Kozlov, G. V. (2000). Structure and properties of polymers in terms of the fractal approach. *Russian Chemical Reviews, 69*(6), 523-549.

34. Munakata, F., Ogiya, T., & Sato, Y. (2024). Thermal conductivities and complex network properties of fractal self-assembled/self-organized texture in binary composite materials. *Applied Physics A, 130*(7), 522.
35. Roman, H. E. (2024). Polymers in physics, chemistry and biology: behavior of linear polymers in fractal structures. *Polymers, 16*(23), 3400.
36. Bronskaya, V. V., Garifullina, E. V., Ignashina, T. V., Aminova, G. A., Manuyko, G. V., Kharitonova, O. S., & Balzamov, D. S. (2022, February). Calculation of the main characteristics of polymer branching taking into account the exchange of activity between polymerization centres. In *IOP Conference Series: Earth and Environmental Science* (Vol. 981, No. 4, p. 042023). IOP Publishing.
37. Zheng, Y., Li, S., Weng, Z., & Gao, C. (2015). Hyperbranched polymers: advances from synthesis to applications. *Chemical Society Reviews, 44*(12), 4091-4130.
38. Rathgeber, S., Pakula, T., Wilk, A., Matyjaszewski, K., & Beers, K. L. (2005). On the shape of bottle-brush macromolecules: Systematic variation of architectural parameters. *The Journal of Chemical Physics,* 122(12), 124904, 13 pages, http://dx.doi.org/10.1063/1.1860531.
39. Phillips, J. C. (1970). Ionicity of the chemical bond in crystals. *Reviews of modern physics, 42*(3), 317.
40. Wunderlich, B. (1992) Heat Capacity of Solid Polymers, in "Thermal Analysis in Metallurgy." edited by R. D. Shull and A. Joshi, *Proc. of the TMS Meeting in Anaheim, CA 1991, The Minerals, Metals and Materials Soc., 2,* 77 – 91.
41. Schliesser, J. M., & Woodfield, B. F. (2015). Lattice vacancies responsible for the linear dependence of the low-temperature heat capacity of insulating materials. *Physical Review B, 91*(2), 024109.
42. Pyda, M., & Wunderlich, B. (1997). Computation of heat capacities of solid state benzene, p-oligophenylenes and poly-p-phenylene. *Journal of Thermal Analysis and Calorimetry, 49*(2), 685-692.
43. Zhang, G., & Wunderlich, B. (1997). Heat capacity of solid-state proteins: I. Thermal analysis. Journal of Thermal Analysis and Calorimetry, 49(2), 823-829.
44. Di Lorenzo, M. L., Zhang, G., Pyda, M., Lebedev, B. V., & Wunderlich, B. (1999). Heat capacity of solid-state biopolymers by thermal analysis. *Journal of Polymer Science Part B: Polymer Physics, 37*(16), 2093-2102.
45. Gaur, U., & Wunderlich, B. (1981). Heat capacity and other thermodynamic properties of linear macromolecules. II. Polyethylene. *Journal of Physical and Chemical Reference Data, 10*(1), 119-152.
46. Gaur, U., Wunderlich, B. B., & Wunderlich, B. (1983). Heat capacity and other thermodynamic properties of linear macromolecules. VII. Other carbon backbone polymers. *Journal of Physical and Chemical Reference Data, 12*(1), 29-63.
47. Gaur, U., Lau, S. F., Wunderlich, B. B., & Wunderlich, B. (1983). Heat capacity and other thermodynamic properties of linear macromolecules. VIII. Polyesters and polyamides. *Journal of Physical and Chemical Reference Data, 12*(1), 65-89.
48. Smirnova, N. N., Kandeev, K. V., Markin, A. V., Bykova, T. A., Kulagina, T. G., & Fainleib, A. M. (2006). Thermodynamics of linear polyurethanes on basis of 1, 4-diisocyanatobutane with 1, 4-butanediol and 1, 6-hexanediol in the range from T→ 0 to 490 K. *Thermochimica acta, 445*(1), 7-18.
49. Gaur, U., Lau, S. F., Wunderlich, B. B., & Wunderlich, B. (1982). Heat capacity and other thermodynamic properties of linear macromolecules VI. Acrylic polymers. *Journal of Physical and Chemical Reference Data, 11*(4), 1065-1089.
50. Gaur, U., & Wunderlich, B. (1981). Heat capacity and other thermodynamic properties of linear macromolecules. IV. Polypropylene. *Journal of Physical and Chemical Reference Data, 10*(4), 1051-1064.
51. Gaur, U., & Wunderlich, B. (1981). Heat capacity and other thermodynamic properties of linear macromolecules. IV. Polypropylene. *Journal of Physical and Chemical Reference Data, 10*(4), 1051-1064.
52. Zhou, J., Chen, C., Sun, J., Fielitz, T. R., Zhou, W., Cahill, D. G., & Braun, P. V. (2025). Reduction of the thermal conductivity of polyurethanes by fluorination: impact of crystallinity, atomic density, and sound velocity. *Angewandte Chemie, 137*(25), e202503497.
53. Ligatchev, V. (2023). Harmonic and anharmonic lattice thermal capacities of molecular wires and 0001-oriented cylindrical ZnO nano-wires. *J. Nanosci. Res. Rep*. 5: 1–10 (2023), DOI: doi.org/10.47363/JNSRR/2023(5)155.
54. Ligatchev, V. (2023). Harmonic and anharmonic lattice thermal capacities of molecular wires and cylindrical ZnO nano-wires. Chapter in: *Prime archives in physical sciences*. Hyderabad, India: Vide Leaf; 1 – 39. doi:1037247.
55. Stephens, R. B., Cieloszyk, G. S., & Salinger, G. L. (1972). Thermal conductivity and specific heat of non-crystalline solids: Polystyrene and polymethyl methacrylate. *Physics Letters A, 38*(3), 215-217.
56. Ligatchev, V. (2020). The 'Generalized Skettrup Model 'and lattice thermal capacity of graphene, h-BN, MoS2, and WS2 Flakes. *ECS J Solid State Sci Technol*. 9(9): 093014. doi: 10.1149/2162-8777/abba04.
57. Blanc, C., Rajabpour, A., Volz, S., Fournier, T., & Bourgeois, O. (2013). Phonon heat conduction in corrugated silicon nanowires below the Casimir limit. *Applied Physics Letters, 103*(4).
58. Pauling, L. (1932). The nature of the chemical bond. IV. The energy of single bonds and the relative electronegativity of atoms. *Journal of the American Chemical Society, 54*(9), 3570-3582.
59. Martoňák, R., Paul, W., & Binder, K. (1998). Orthorhombic phase of crystalline polyethylene: A constant pressure path-integral

Monte Carlo study. *Physical Review E, 57*(2), 2425.
60. Wigner, E. (1932). On the quantum correction for thermodynamic equilibrium. *Physical review, 40*(5), 749.
61. Kirkwood, J. G. (1933). Quantum statistics of almost classical assemblies. *Physical Review, 44*(1), 31.
62. Mondescu, R. P., & Muthukumar, M. (1998). Brownian motion and polymer statistics on certain curved manifolds. *Physical Review E, 57*(4), 4411.
63. Huang, J., Li, S., Zhang, X., & Huang, G. (2020). Neural network model for structure factor of polymer systems. *The Journal of Chemical Physics, 153*(12), 124902, htpps://doi.org/10.1063/5.0022464.